A numerical support of leading point concept

Available online at www.sciencedirect.com

ScienceDirect

journal homepage: www.elsevier.com/locate/he

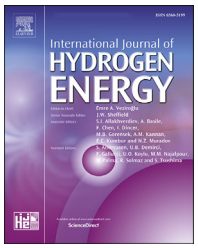

A numerical support of leading point concept

Hsu Chew Lee [a,b], *Peng Dai* [a], *Minping Wan* [a,b], *Andrei N. Lipatnikov* [c,*]

[a] *Guangdong Provincial Key Laboratory of Turbulence Research and Applications, Department of Mechanics and Aerospace Engineering, Southern University of Science and Technology, Shenzhen 518055, China*

[b] *Guangdong-Hong Kong-Macao Joint Laboratory for Data-Driven Fluid Mechanics and Engineering Applications, Southern University of Science and Technology, Shenzhen 518055, China*

[c] *Department of Mechanics and Maritime Sciences, Chalmers University of Technology, Gothenburg SE-412 96, Sweden*

HIGHLIGHTS

- Crucial role played by the leading edge of a premixed turbulent flame brush is evidenced.
- Preferential diffusion of H_2 significantly accelerates even highly turbulent lean H_2-air flames.
- This effect is significantly more pronounced in leaner flames.
- Preferential diffusion of H weakly affects burning velocity of such flames.

ARTICLE INFO

Article history:
Received 6 January 2022
Received in revised form
24 April 2022
Accepted 15 May 2022
Available online 5 June 2022

Keywords:
Turbulent combustion
Leading point concept
Preferential diffusion
Lewis number
Turbulent burning velocity
Hydrogen

ABSTRACT

Unsteady three-dimensional Direct Numerical Simulation (DNS) data obtained from 16 statistically planar and one-dimensional, complex-chemistry, lean (equivalence ratio is equal to 0.50 or 0.35) hydrogen-air flames propagating in forced, intense, small-scale turbulence (Karlovitz number up to 565) are reported. The data are analyzed to compare roles played by leading and trailing edges of a premixed turbulent flame brush in its propagation. The comparison is based on the following considerations: (i) positively (negatively) curved reaction zones predominate at the leading (trailing, respectively) edge of a premixed turbulent flame brush and (ii) preferential diffusion of molecular or atomic hydrogen results in increasing the local fuel consumption and heat release rates in positively or negatively, respectively, curved reaction zones. Therefore, turbulent burning velocities computed by deactivating differential diffusion effects for all species with the exception of either H_2 or H are compared for assessing roles played by leading and trailing edges of a premixed turbulent flame brush in its propagation. By analyzing the DNS data, a significant increase in the local fuel consumption and heat release rates due to preferential diffusion of H_2 or H is documented close to the leading or trailing, respectively, edges of the studied flame brushes. Nevertheless, turbulent burning velocities computed by activating preferential diffusion solely for H_2 are significantly higher than turbulent burning velocities computed by activating preferential diffusion solely for H. This result indicates an important role played by the leading edge in the propagation of the explored turbulent flame brushes.

* *Corresponding author.*
E-mail address: lipatn@chalmers.se (A.N. Lipatnikov).

https://doi.org/10.1016/j.ijhydene.2022.05.140

Introduction

Energy demand has shown no sign of slowing down and is expected to increase further in the near foreseeable future due to an increase in the world population and the rapid rise in living standards outside developed countries [1]. Hence, there is an urgent need to decrease or rather eliminate our heavy reliance on fossil fuels for most of our energy demands, especially, because the usage of fossil fuels is often considered to substantially contribute to climate changes [2] that our Earth could no longer withstand without inducing irreversible consequences for future generations to come. From this perspective, hydrogen is widely recognized to be a promising renewable and carbon-free energy source capable for replacing fossil fuels in future engines and power plants [2–5].

The possibility of using hydrogen as a sustainable fuel in combustion engines was reviewed by many experts, e.g., see Refs. [2,4,6–10]. These authors highlighted the need to substantially improve our understanding of physics of hydrogen combustion in order to significantly accelerate adoption of H_2 as a renewable, carbon-free fuel. Since experimental investigation of hydrogen flames is expensive and challenging [11–14], Computational Fluid Dynamics (CFD) tools could significantly facilitate R&D of future ultra-clean and highly efficient hydrogen combustion technologies. Accordingly, there is a growing body of studies aiming at modeling combustion of hydrogen [15–24].

However, the utility of CFD tools for research into burning of H_2 in engines and power plants is strongly limited by inability of the vast majority of contemporary models of turbulent combustion, implemented into commonly used CFD software, to predict abnormally high ratios S_t/S_L of turbulent and laminar flames speeds, which are well documented by various research groups in a number of experiments with lean hydrogen-air mixtures, e.g., see Refs. [25–33], as well as a review article [34] or a book [35]. The present authors are aware of a single successful attempt [36,37] to compute appropriately high values of S_t/S_L for lean H_2-air flames, with this result being obtained by adapting a leading point concept of turbulent burning.

In the combustion science, the concept was pioneered by the Russian school, as reviewed elsewhere [38,39]. The concept is based not only on physical reasoning, but also on a general theory of convection-diffusion-reaction (CDR) equations, which are widely used in various fields of science. Mathematical research into such a class of partial differential equations was pioneered by Fisher [40] and Kolmogorov et al. [41] who studied biological problems. In particular, Kolmogorov et al. [41] rigorously proved the seminal KPP (Kolmogorov, Petrovsky and Piskounov) theorem, which yielded an analytical expression for the speed of the physically realizable traveling-wave solution to a CDR equation whose source (reaction) term satisfied certain constraints. The key consequence of the KPP theorem consists in predicting the crucial role played by the leading edge of a traveling wave in its propagation. More specifically, the aforementioned physically realizable traveling-wave speed is controlled by the behavior of the reaction (source) term at the leading edge [41] but is not affected by variations of this term within the wave. Such traveling waves are called pulled waves [42,43]. Subsequent applications and development of the KPP theory in mathematical biology and other fields of science were reviewed, e.g., by Murray [44,45], Ebert and van Saarloos [42], and van Saarloos [43].

The KPP theory was also invoked for modeling premixed turbulent burning [46–54]. Moreover, the theory laid mathematical foundations for the leading point concept of premixed turbulent flames. As already noted, an important peculiarity of the concept consists of its capability for predicting [36,37] the abnormally high ratios S_t/S_L, which are well documented in lean hydrogen-air and lean syngas-air mixtures [25–35]. This advantage of the concept appears to be of great importance due to rapidly growing interest in developing combustion engines fueled with hydrogen [4–10]. Over the recent years, the concept was supported in experimental [31,32,55], theoretical [56–58], and numerical, both Direct Numerical Simulation (DNS) [59–61] and Reynolds-Averaged Navier-Stokes (RANS) simulation [62], studies.

Nevertheless, neither the cited papers nor the KPP theory prove that propagation of a premixed turbulent flame is controlled by processes localized to its leading edge. The point is that the KPP theory addresses a wide, but bounded class of source term shapes in CDR equations, whereas the source term shape, e.g., dependence of mean heat release rate on mean species concentrations and temperature, is not known *a priori* for a premixed turbulent flame. There are alternative model expressions, e.g., see Refs. [49,63], but none of them is rigorous. For the same reasons, results of studies of CDR equations with source terms that do not satisfy the KPP constraints, e.g., see Refs. [57,64,65], do not allow us to rigorously prove validity of the leading point concept either.

Moreover, in various fields of science, there are known traveling waves whose speeds are controlled by processes localized to their trailing edges [64,66]. Such waves are called pushed waves [42,43]. In the combustion science, a laminar premixed flame described by the ZFK (Zel'dovich and Frank-Kamenetskii) theory [38,67] is a well-known example of a pushed traveling wave. Transition from pushed to pulled flames was also demonstrated by changing the shapes of source terms in CDR equations [57,66,68–71]. Furthermore, significant influence of processes localized to the trailing edge of a turbulent flame brush on its speed was revealed in recent DNS studies of burning of highly preheated mixtures [72,73]. Under conditions of these simulations, molecular diffusion of atoms H into negatively curved cusps promoted local autoignitions in the trailing zones of the studied turbulent flames, thus, significantly accelerating their propagation [73] in line with Zel'dovich's prediction [69] of spontaneous propagation of chemical reactions due to a spatial gradient of ignition time, caused by local mixture non-uniformities.

Thus, despite a growing body of indirect evidence in favor of the leading point concept [31,32,55–62], at least in lean flames of H_2 or H_2-containing fuel blends, the hypothesis on the crucial role played by the leading edge of such flames in their propagation still requires further study. In particular, not only this crucial role should be confirmed, but also conditions under that premixed turbulent flames are pulled waves should be explored. The present work aims at partially bridging this knowledge gap by developing a simple numerical

method for comparing roles played by the leading and trailing edges of a lean hydrogen-air turbulent flame brush in its propagation.

The method and DNS data that the method is applied to are discussed in the next section. Numerical results are presented and analyzed in the third section followed by conclusions. It is worth stressing that while the reported DNS data show several interesting effects, the present communication is solely restricted to the major goal stated above (comparing roles played by the leading and trailing edges of a lean hydrogen-air turbulent flame brush in its propagation), whereas other observed effects will be analyzed in subsequent papers.

Methodology

Key points

First, from the theory of perturbed single-step-chemistry laminar flames [38,74,75], it is well-known that the fuel concentration and temperature are locally increased (decreased) in positively (negatively) curved reaction zones if the Lewis number $Le = a/D_d$ is less than unity. Here, a is the molecular heat diffusivity of the considered fuel-air mixture; D_d is the molecular diffusivity of the deficient reactant in the mixture, e.g., the molecular diffusivity of H_2 in a lean hydrogen-air flame, where $Le < 1$; and the curvature is positive if its center is in products, e.g., in expanding cylindrical or spherical laminar flames. Both an increase in the local temperature in positively curved reaction zones and an increase in the local equivalence ratio (or/and temperature) in such zones were documented in DNS studies of single-step chemistry low Le premixed turbulent flames [76,77] and lean complex chemistry hydrogen-air [78–84] or H_2/NH_3/-air [73] turbulent flames.

Second, in a lean complex-chemistry hydrogen-air flame, not only molecular, but also atomic hydrogen is characterized by high molecular diffusivity. Accordingly, via an analogy with H_2, the local concentration of H is also expected to vary significantly in curved reaction zones due to differential diffusion effects. However, there is an important difference between spatial variations of H_2 and H in premixed flames. While the concentration of molecular hydrogen peaks upstream of a reaction zone, the concentration of atomic hydrogen peaks downstream of the zone, i.e., in a radical recombination zone [85]. Therefore, the differential diffusion effects are expected to increase (decrease) the local concentration of H in negatively (positively, respectively) curved reaction zones. This phenomenon was indeed documented in recent DNS studies [73,81,82,84]. In particular, Rieth et al. [73] analyzed DNS data obtained from (i) highly preheated statistically planar lean H_2-air turbulent flames and (ii) preheated lean NH_3/H_2/air flames propagating in turbulent shear layers. The reported results do show that molecular diffusion of H into negatively curved heat release zones can cause a significant increase in the local concentration of atomic hydrogen and heat release rate [73].

Thus, on the one hand, differential diffusion effects are expected to increase the local concentration of molecular (atomic) hydrogen in positively (negatively) curved reaction zones, thus, increasing the local fuel consumption (heat release) rate. On the other hand, for purely topological reasoning, the probability of finding positively (negatively) curved reaction zones is expected to be higher at the leading (trailing, respectively) edge of a premixed turbulent flame brush. Such a trend was earlier documented in experimental [86–88] and DNS [87,89,90] studies, see also fig. 8b in Ref. [91] as a recent example. Therefore, preferential diffusion of molecular (atomic) hydrogen is expected to increase the local fuel consumption and/or heat release rate at the leading (trailing, respectively) edge of a lean hydrogen-air turbulent flame brush. Consequently, if molecular diffusivities D_k are set equal to the heat diffusivity a for all species k with the exception of molecular (atomic) hydrogen, preferential diffusion of H_2 (H, respectively) should increase turbulent burning velocity U_t provided that processes localized to the leading (trailing, respectively) edge of the flame brush substantially affect U_t. Thus, comparison of turbulent burning velocities computed in the cases of (i) $D_k = a$ for all species with the exception of $D_H > a$ and (ii) $D_k = a$ for all species with the exception of $D_{H_2} > a$ offers an opportunity to compare roles played by the trailing and leading edges of a lean hydrogen-air turbulent flame brush in its propagation. This simple idea is implemented in the present study. In the following, cases (i) and (ii) will be labeled using symbols 1H and 1H2, respectively.

Direct numerical simulations

Since the DNS setup and numerical methods were already described elsewhere [84,92,93], we will restrict ourselves to a brief summary of the adopted numerical approach. Unconfined statistically planar and one-dimensional lean hydrogen-air flames propagating in a forced turbulence under the room conditions were simulated by invoking a detailed chemical mechanism (22 reactions and 9 species) by Kéromnès et al. [94] and adopting the solver *DINO* [95] to numerically integrate unsteady three-dimensional transport and Navier-Stokes equations in the low-Mach-number formulation. Turbulent inflow and outflow boundary conditions were set along the streamwise y-direction. Along the spanwise and transverse x and z-directions, respectively, the boundary conditions were periodic. The computational domain $\Lambda \times 16\Lambda \times \Lambda$ was discretized using a uniform Cartesian grid of $N_x \times 16N_x \times N_x$ cells.

Unburned reactants were injected into the computational domain through the left boundary $y = 0$. To ensure a positive inlet velocity, the inlet flow was laminar. Inside the computational domain, turbulence was generated by adopting the linear forcing method [96,97] in a layer of $0.5\Lambda \leq y \leq 8\Lambda$. As discussed in detail earlier [84, fig. 2a], the transverse-averaged turbulent kinetic energy $\langle k \rangle(y,t)$ was almost independent of time t or axial distance y both before and after embedding a laminar flame into the flow, i.e., $\langle k \rangle(y,t) \approx k_0$. Similarly, the transverse-averaged dissipation rate $\langle \varepsilon \rangle(y,t) \approx \varepsilon_0$, but only before embedding the flame into the flow. During combustion phase, $\langle \varepsilon \rangle(y,t)$ decreased with y [84, fig. 2b] due to an increase in the flow length scales, caused by thermal expansion. In a

single case, simulations were also performed by switching off turbulence generation and allowing the turbulence to decay in time, with all other things being equal. As discussed in detail elsewhere [84], such a change of turbulence evolution weakly affected major trends highlighted in Refs. [84,92].

The simulation conditions are summarized in Table 1, where u' and $L = u'^3/\varepsilon_0$[84] are the rms turbulent velocity and an integral length scale, respectively; $Re_t = u'L/\nu_u$ is the turbulent Reynolds number; $\eta = LRe_t^{-3/4}$ is the Kolmogorov length scale; ν_u is the kinematic viscosity of unburned mixture; ϕ is the equivalence ratio; $\delta_L^T = (T_b - T_u)/\max\{|dT/dx|\}$, S_L, and $\tau_f = \delta_L^T/S_L$ are the laminar flame thickness, speed, and time scale, respectively; $Ka = (u'/S_L)^{3/2}(\delta_L^T/L)^{1/2}$ and $Da = \tau_t/\tau_f$ are the Karlovitz and Damköhler numbers, respectively; Δx is the grid size; T is the temperature; subscripts u and b designate unburnt reactants and equilibrium combustion products, respectively. The sole difference between cases $\mathscr{D}$ and $\mathscr{D}1$, where $\mathscr{D}$ designates a capital letter (C, D, E, or F), consists of substitution of mixture-averaged molecular diffusivities $D_k \neq a$, calculated using code *Cantera* [98] (cases $\mathscr{D}$), with $D_k = a$ for all species k (cases $\mathscr{D}1$). In case $\mathscr{D}1$H or $\mathscr{D}1$H2, the same mixture averaged $D_H > a$ or $D_{H_2} > a$ was adopted, respectively, with $D_k = a$ for all other species. In line with the theory of laminar premixed flames [38], cases $\mathscr{D}1$ are characterized by a higher laminar flame speed S_L when compared to cases $\mathscr{D}$.

Results obtained in C-set of four cases were analyzed in our earlier paper [93]. Twelve new cases were designed to explore effects due to variations in the equivalence ratio, u'/S_L, and L/δ_L^T. More specifically, flames C and D propagate in the statistically same turbulence, but are characterized by different ϕ and, hence, by different S_L, δ_L^T, or τ_f. Accordingly, the values of u'/S_L, L/δ_L^T, Da, or Ka are also different for each pair of counterpart cases from C and D families. Flames D and E are characterized by different rms turbulent velocities, with all other things being equal. More specifically, the rms velocity is decreased in case E in order for the ratios of u'/S_L to be approximately equal in cases C and E, characterized by different equivalence ratios and still different L/δ_L^T, Da, or Ka. Finally, in F-set of cases, the computational domain width Λ and turbulence length scale L are increased in order for the values of u'/S_L, L/δ_L^T, Da, or Ka to be approximately equal in flames C and F. Therefore, the value of ϕ is the major difference between these two flames. Among 16 simulated cases, flame D is characterized by the highest Karlovitz number and the lowest Damköhler number, see Table 1.

While this DNS database was created to explore several issues, the following discussion will solely be restricted to the major goal of the present work, i.e., comparison of contributions from leading and trailing edges of turbulent flame brushes to burning velocities. Accordingly, the focus of discussion will be placed on cases $\mathscr{D}1$H and $\mathscr{D}1$H2. Other cases and other effects found by analyzing the entire DNS database will be addressed in subsequent papers.

When processing the DNS data, the combustion progress variable $c_F = (Y_{H_2,u} - Y_{H_2})/Y_{H_2,u}$ was defined using the fuel mass fraction Y_{H_2}; the local equivalence ratio was calculated as follows

$$\phi = \frac{1}{2}\frac{2X_{H_2} + 2X_{H_2O} + X_H + X_{OH} + X_{HO_2} + 2X_{H_2O_2}}{2X_{O_2} + X_{H_2O} + X_O + X_{OH} + 2X_{HO_2} + 2X_{H_2O_2}}; \quad (1)$$

time-dependent turbulent burning velocities were equal to

$$U_t^F(t) = -\frac{1}{(\rho Y_{H_2})_u L_x^2}\iint_\Omega \dot{\omega}_{H_2}(\mathbf{x},t)d\mathbf{x}, \quad (2)$$

$$U_t^T(t) = \frac{1}{L_x^2}\iint_\Omega \frac{\dot{W}_T(\mathbf{x},t)}{c_p(T_b - T_u)}d\mathbf{x}; \quad (3)$$

and averaging (conventional or conditioned) was performed across transverse planes $y = \text{const}$, with $\langle q\rangle(y,t)$ designating instantaneous transverse-averaged value of the quantity q. Here, X_S is the mole fraction of species S; $\dot{W}_T = \sum_{k=1}^{N} h_k\dot{\omega}_k$ is the

Table 1 – Studied cases.

Cases	ϕ	S_L, m/s	δ_L^T, mm	u'/S_L	L/δ_L^T	Da	Ka	Re_t	$\Delta x/\delta_L^T$	$\Delta x/\eta$	N_x	Λ, mm
C	0.5	0.58	0.41	11.8	1.1	0.10	33.0	158	0.045	1.85	128	2.4
C1	0.5	0.78	0.29	8.3	1.6	0.19	19.0	158	0.066	1.85	128	2.4
C1H	0.5	0.91	0.34	7.1	1.4	0.19	16.6	158	0.057	1.85	128	2.4
C1H2	0.5	0.51	0.34	12.7	1.4	0.10	39.4	158	0.057	1.85	128	2.4
D	0.35	0.12	0.92	54	0.5	0.009	565	160	0.021	1.85	128	2.4
D1	0.35	0.30	0.43	22	1.1	0.05	97	160	0.045	1.85	128	2.4
D1H	0.35	0.27	0.54	24	0.8	0.04	126	160	0.033	1.85	128	2.4
D1H2	0.35	0.175	0.64	37	0.7	0.02	268	160	0.029	1.85	128	2.4
E	0.35	0.12	0.92	11.2	0.5	0.04	53	33	0.021	1.13	64	2.4
E1	0.35	0.30	0.43	4.5	1.1	0.24	9.1	33	0.045	1.13	64	2.4
E1H	0.35	0.27	0.54	4.9	0.8	0.17	12	33	0.033	1.13	64	2.4
E1H2	0.35	0.175	0.64	7.7	0.7	0.09	25	33	0.029	1.13	64	2.4
F	0.35	0.12	0.92	11.2	1.15	0.10	35	77	0.047	1.07	128	5.6
F1	0.35	0.30	0.43	4.5	2.5	0.56	6.0	77	0.103	1.07	128	5.6
F1H	0.35	0.27	0.54	4.9	2.0	0.40	7.8	77	0.082	1.07	128	5.6
F1H2	0.35	0.175	0.64	7.7	1.7	0.22	16.5	77	0.070	1.07	128	5.6

heat release rate; c_p is the specific heat capacity of the mixture; ρ is the mixture density; h_k is the enthalpy of species k; $\dot{\omega}_k$ is the rate of production of species k (note that $\dot{\omega}_{H_2} \leq 0$); integration is performed over the 3D computational domain Ω. Finally, the local mean curvature $\kappa = \nabla \cdot \mathbf{n}/2$, where the unit vector $\mathbf{n} = -\nabla c/|\nabla c|$ is normal to the iso-surface of $c(\mathbf{x}, t) =$ const and points to unburnt mixture.

Unperturbed laminar premixed flames associated with family C and three other families of the DNS cases were simulated (i) using the same chemical mechanism [94] and mixture-averaged molecular diffusivities for all species and (ii) running code *Cantera* [98]. Shown in Fig. 1 are the normalized fuel consumption rates $\dot{\omega}_{F,L}(c_F)$ (left column) and heat release rates $\dot{W}_{T,L}(c_F)$ (right column) obtained from lean ($\phi = 0.5$, top row) and very lean ($\phi = 0.35$, bottom row) unperturbed laminar flames under the room conditions. The rates are normalized using their peak values $\dot{\omega}_{F,L,max}$ and $\dot{W}_{T,L,max}$ in flames C or D. The laminar flame speeds and thicknesses, reported in Table 1, have been obtained in such simulations.

Results and discussion

Before comparing turbulent burning velocities computed in cases $\mathscr{D}$1H and $\mathscr{D}$1H2, let's first explore the key points emphasized earlier. Fig. 2 confirms that the probability $P(\delta_L^T \kappa > 1)$ of finding highly and positively curved reactions zones peaks at low values of temporally and transverse-averaged combustion progress variable $\bar{c}_F$ and decreases with increasing $\bar{c}_F$, see black lines, whereas the probability $P(\delta_L^T \kappa < -1)$ of finding highly and negatively curved reactions zones is increased by $\bar{c}_F$, see red lines, and peaks close to the trailing edge. These results are consistent with earlier studies [86–91]. The increase in $P(\delta_L^T \kappa < -1)$ by $\bar{c}_F$ is less pronounced than the decrease in $P(\delta_L^T \kappa > 1)$ with $\bar{c}_F$. At $\bar{c}_F = 0.95$, the former probability is significantly larger than the latter one in cases C, D, and E, whereas the two probabilities are close to one another in case F, see dotted lines.

Shown in Fig. 3 are time averaged conditioned profiles of equivalence ratio (top row), temperature (middle row), and

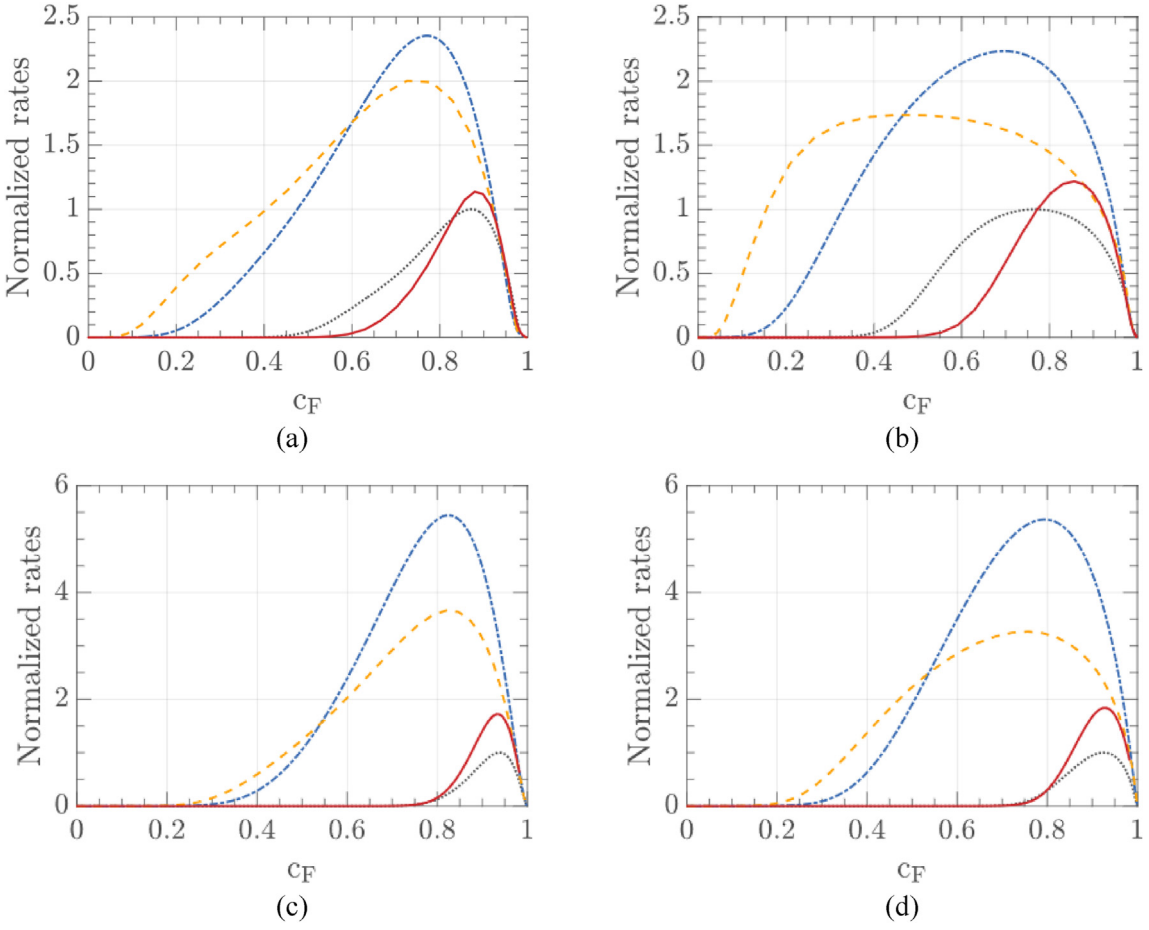

Fig. 1 – Profiles of normalized (a, c) fuel consumption and (b, d) heat release rates in the unperturbed laminar flames characterized by (a, b) $\phi = 0.5$ and (c, d) $\phi = 0.35$. The rates are normalized using their peak values computed in the laminar counterparts of case C or D. Results obtained from the laminar counterparts of cases C or D, C1 or D1, C1H or D1H, and C1H2 or D1H2 are plotted in black dotted, blue dotted-dashed, yellow dashed, and red solid lines, respectively. (For interpretation of the references to color in this figure legend, the reader is referred to the Web version of this article.)

mass fraction of atomic hydrogen (bottom row), re-normalized using the peak value of Y_H in the laminar counterpart of flame C characterized by $\phi = 0.5$. Results reported in the left and right columns have been sampled from the leading and trailing zones of flame brushes in C-set of cases. These zones are defined with $\langle c_F \rangle(y,t) = 0.1 \pm 0.05$ and $c_F(y,t) = 0.9 \pm 0.05$, respectively. As expected in the case of $D_{H_2} = D_{O_2}$, variations in the conditioned equivalence ratio are weakly pronounced in flames C1 and C1H, see blue dotted-dashed and yellow dashed lines, respectively, in Fig. 3a and b. On the contrary, the local equivalence ratio is significantly increased (decreased) in reaction zones close to the leading (trailing, respectively) edges of flame brushes in cases C and C1H2. These effects are associated with an increased (decreased) molecular flux of H_2 from unburned reactants to positively (negatively, respectively) curved reaction zones localized predominantly to the leading (trailing, respectively) edges. Note that profiles of $\langle \phi | c_F \rangle (c_F)$ obtained from flames C and C1H2 are very close to one another, thus, indicating that the local variations in the equivalence ratio are mainly controlled by the molecular diffusivity of H_2.

Profiles of $\langle T | c_F \rangle (c_F)$, reported in Fig. 3c and d, are basically similar to the profiles of $\langle \phi | c_F \rangle (c_F)$, discussed earlier. In positively (negatively) curved fuel consumption zones ($c_F > 0.4$) concentrated to the leading (trailing, respectively) edge, the local temperature is increased (decreased, respectively) in cases C and C1H2 when compared to cases C1 and C1H. These effects are associated not only with the local increase (decrease, respectively) in the equivalence ratio, see Fig. 3a and b, but also (and mainly) with the local increase (decrease, respectively) in the total enthalpy, because molecular flux of chemical energy to positively (negatively, respectively) curved reaction zones overwhelms (is overwhelmed by, respectively) heat losses from these zones if $Le < 1$ [38]. Moreover, comparison of curves plotted in blue dotted-dashed (C1) and yellow dashed (C1H) lines in Fig. 3d indicates that preferential diffusion of H into negatively curved heat release zones concentrated to the trailing edge results in increasing the local temperature. This phenomenon is associated with a substantial increase in the local heat release rate in the low-temperature region of negatively curved heat release zones, explored earlier [73,81,82,84,93] and in Fig. 4d.

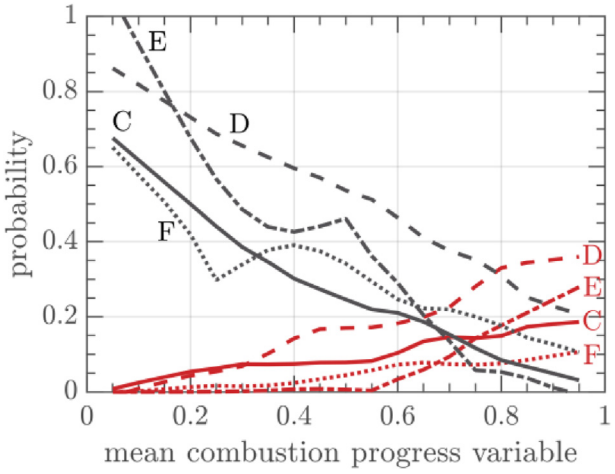

Fig. 2 – Probabilities of finding $\delta_L^T \kappa > 1$ (black lines) and $\delta_L^T \kappa < -1$ (red lines) vs. transverse and time-averaged combustion progress variable $\bar{c}_F(y)$. The probabilities have been sampled from flame zones characterized by a sufficiently high local fuel consumption rate (larger than 5% of its peak value in the studied turbulent flames). Results obtained from flames C, D, E, and F are plotted in solid, dashed, dotted-dashed, and dotted lines, respectively. (For interpretation of the references to color in this figure legend, the reader is referred to the Web version of this article.)

Fig. 3e shows that the concentration of atomic hydrogen in reaction zones close to the leading edge is increased due to preferential diffusion of H_2 to the zones, but is decreased due to preferential diffusion of H. Indeed, $\langle Y_H | c_F \rangle$ is highest in case C1H2 (large D_{H_2} and reduced D_H, red solid line) and lowest in case C1H (reduced D_{H_2} and large D_H, yellow dashed line). If both D_{H_2} and D_H are large (case C, black dotted line), $\langle Y_H | c_F \rangle$ is higher than in case C1 (blue dotted-dashed line) characterized by reduced D_{H_2} and D_H. The opposite trends are observed close to the trailing edge provided that $c_F < 0.6$, see Fig. 3f. An increase in $\langle Y_H | c \rangle$ due to preferential diffusion of atomic hydrogen is most pronounced in the low-temperature region ($c_F < 0.6$), cf. yellow dashed (case C1H) and blue dotted-dashed (case C1) lines.

The trends discussed above explain variations in conditioned fuel consumption and heat release rates close to the leading or trailing edge. Fig. 4a and c shows that preferential diffusion of molecular (atomic) hydrogen results in increasing (decreasing, respectively) the local fuel consumption and heat release rates close to the leading edges, cf. curves plotted in red solid (yellow dashed, respectively) and blue dotted-dashed lines. For instance, the peak conditioned fuel consumption or heat release rate in the turbulent flame C1H2 or C is significantly higher than the peak fuel consumption or heat release rate in the counterpart laminar flame, cf. peaks of curves plotted in red solid or black dotted lines in Figs. 4a and 1a or in Figs. 4c and 1b, respectively. The opposite trend is observed for these rates in the turbulent flame C1H and the counterpart laminar flame, cf. peaks of curves plotted in yellow dashed lines in Figs. 4a and 1a or in Figs. 4c and 1b. In addition, preferential diffusion of atomic hydrogen from products to unburned reactants can increase the local heat release rate in the low-temperature regions [73,81,82], cf. curves plotted in red solid (C1H2, D_H is reduced) and black dotted (C, large D_H) lines in Fig. 4c.

Close to the trailing edge, the local fuel consumption or heat release rates are also increased in the turbulent flames C, C1H, and C1H2 when compared to the counterpart laminar flames, cf. Figs. 4b and 1a or Figs. 4d and 1b, respectively. Fig. 4b shows that the conditioned fuel consumption rate is significantly higher in case C1H (large D_H, yellow dashed line) when compared to case C1H2 (large D_{H_2}, red solid line). A similar effect is observed for the conditioned heat release rates in Fig. 4d, but only if $c_F < 0.7$. The peak conditioned fuel consumption or heat release rate near the trailing edge of the turbulent flame C1H is higher than the peak fuel consumption

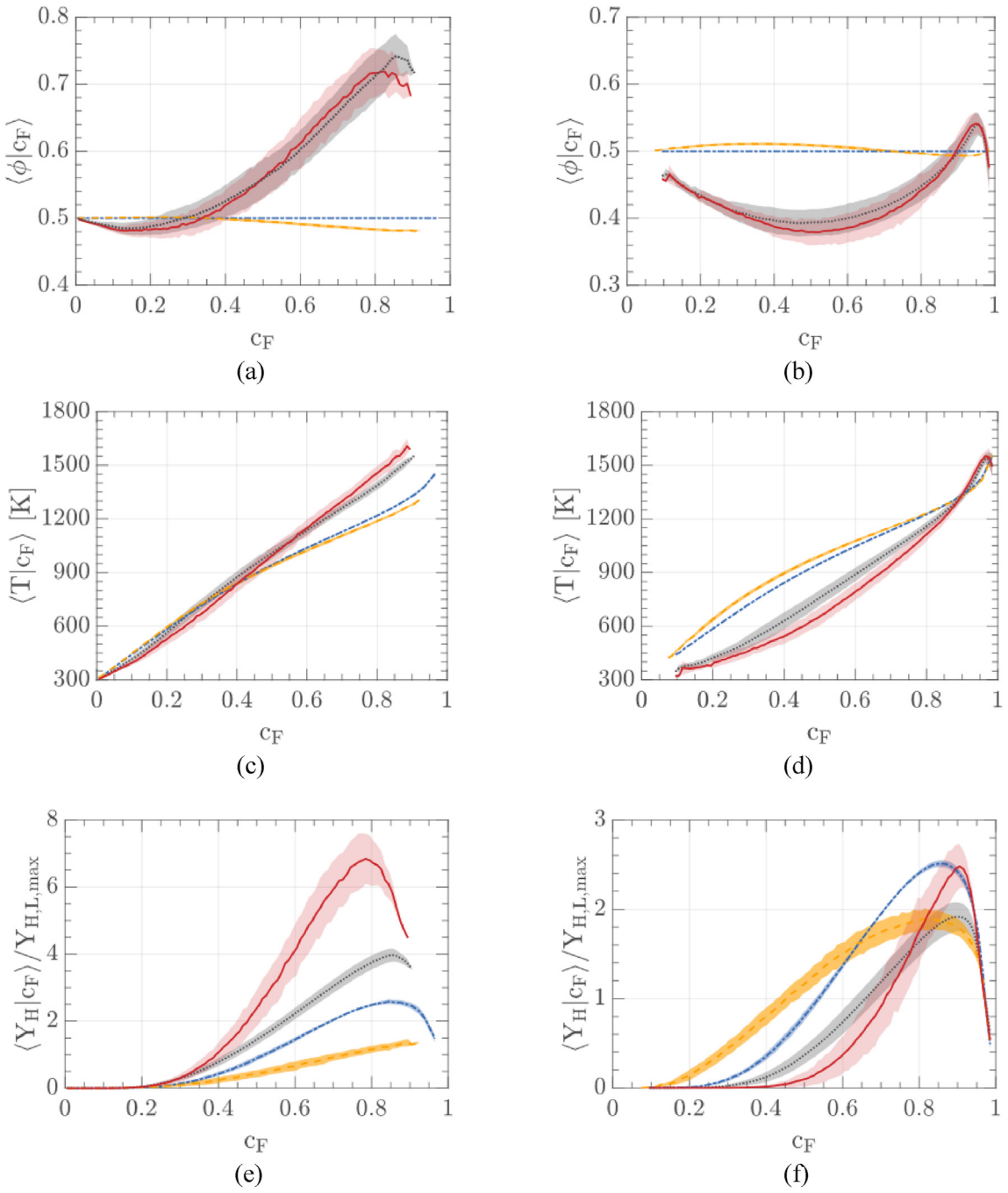

Fig. 3 – Time-averaged conditioned profiles of (a, b) equivalence ratio, (c, d) temperature, and (e, f) re-normalized mass fraction of atomic hydrogen, obtained from leading, i.e., $\langle c_F\rangle(y,t) = 0.1\pm0.05$, and trailing, i.e., $\langle c_F\rangle(y,t) = 0.9\pm0.05$, zones of flame brushes in case C (black dotted lines), C1 (blue dotted-dashed lines), C1H (yellow dashed lines), and C1H2 (red solid lines). Shaded regions show ± rms values. (For interpretation of the references to color in this figure legend, the reader is referred to the Web version of this article.)

or heat release, respectively, rate in the counterpart laminar flame, cf. peaks of curves plotted in yellow dashed lines in Figs. 4b and 1a or 4d and 1b, respectively, but the effect magnitude is relatively low (about 10%).

For the goals of the present study, the most important results are plotted in red solid and yellow dashed lines in Fig. 4. Comparison of these results shows a significant increase in the local fuel consumption and heat release rates due to (i) preferential diffusion of molecular hydrogen close to the leading edges and (ii) preferential diffusion of atomic hydrogen close to the trailing edges. The same trends are documented for three sets of leaner flames, cf. curves plotted in red solid and black dashed lines in Fig. 5 or 6, respectively. Thus, Figs. 4–6 support the key points stated in the second

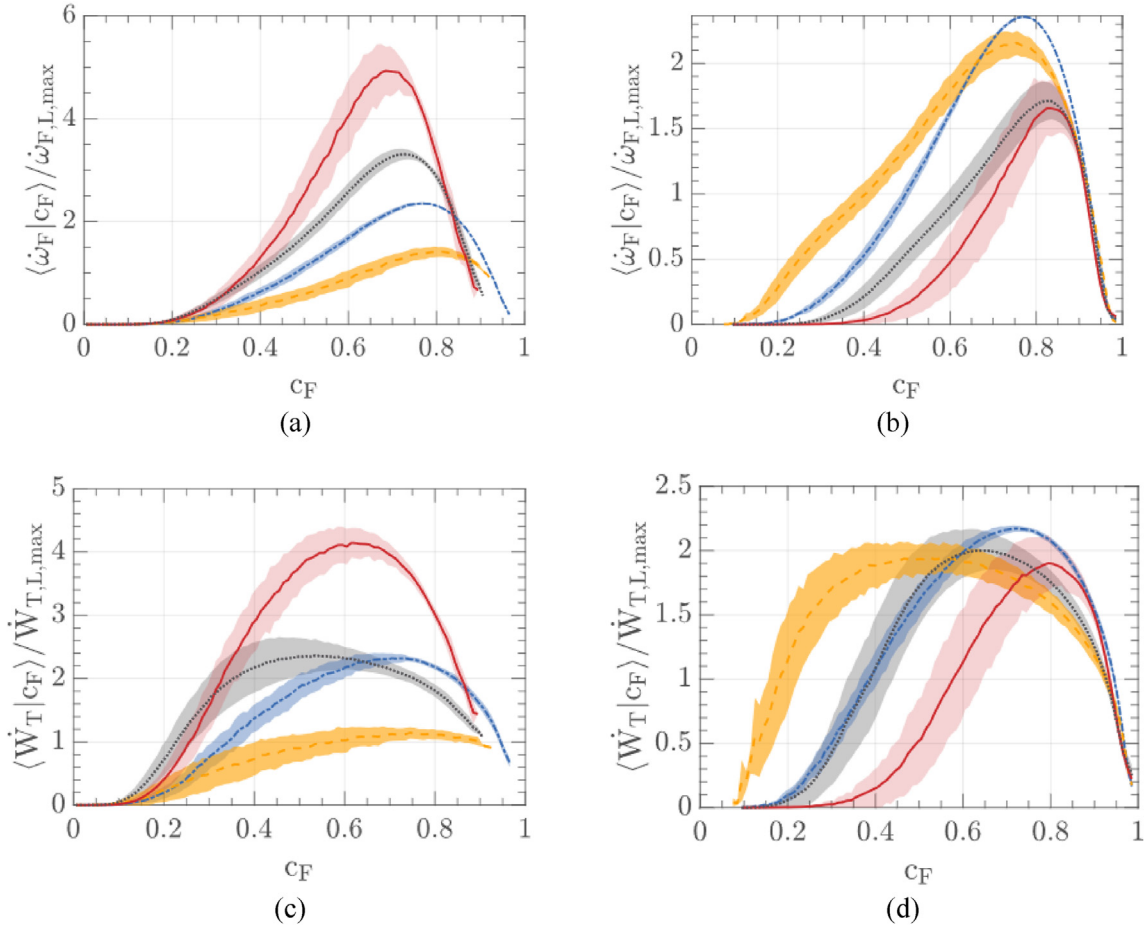

Fig. 4 – Time-averaged conditioned profiles of normalized (a–b) fuel consumption and (c–d) heat release rates, obtained from the (a, c) leading and (b, d) trailing zones of flame brushes in case C (black dotted lines), C1 (blue dotted-dashed lines), C1H (yellow dashed lines), and C1H2 (red solid lines). The rates are normalized using their peak values in the unperturbed laminar flame characterized by $\phi = 0.5$. Shaded regions show ± rms values. (For interpretation of the references to color in this figure legend, the reader is referred to the Web version of this article.)

section and suggest comparing turbulent burning velocities computed in cases $\mathscr{D}$1H or $\mathscr{D}$1H2 in order to assess a role played by the trailing or leading edge of a premixed turbulent flame brush in its propagation.

Evolutions of turbulent burning velocities evaluated using Eqs. (2) and (3) are shown in Figs. 7 and 8, respectively. The time-averaged turbulent burning velocities are reported in Table 2. These values were averaged when the normalized time $t^* = t/\tau_t$ was larger than 15, 6, 10, and 4 in sets C, D, E, and F, respectively. All these results clearly show that preferential diffusion of atomic hydrogen weakly affects turbulent burning velocity, cf. cases $\mathscr{D}$1H and $\mathscr{D}$1, whereas preferential diffusion of molecular hydrogen results in significantly increasing U_t^F or U_t^T, cf. cases $\mathscr{D}$1H2 and $\mathscr{D}$1. For all four families of cases, the turbulent burning velocities are significantly higher in flame $\mathscr{D}$1H2 when compared to $\mathscr{D}$1H, cf. curves plotted in red solid and yellow dashed lines in Figs. 7 or 8. The computed increase in U_t^F or U_t^T in cases $\mathscr{D}$ when compared to $\mathscr{D}$1, cf. curves plotted in black dotted and blue dotted-dashed lines, is mainly controlled by the preferential diffusion of molecular hydrogen.

Thus, on the one hand, Figs. 4–8 show that the high diffusivity of H_2 results in significantly increasing both (i) fuel consumption and heat release rates at the flame-brush leading edges and (ii) turbulent burning velocity (cf. cases $\mathscr{D}$1 and $\mathscr{D}$1H2). On the other hand, Figs. 4–8 show that the high diffusivity of H results in (i) significantly increasing fuel consumption and heat release rates at the trailing edge (cf. cases $\mathscr{D}$1H and $\mathscr{D}$1 or $\mathscr{D}$1H2), but (ii) weakly affects turbulent burning velocity (cf. cases $\mathscr{D}$1 and $\mathscr{D}$1H). These findings considered together evidence that the leading (trailing) edge plays an important (minor, respectively) role in turbulent flame propagation. While these findings are fully consistent with the leading point concept [34–39], they do not prove it rigorously.

Accordingly, to further support the concept, Fig. 9 reports time-averaged conditioned profiles of normalized fuel consumption rate, sampled from (a) entire flame brushes or (b) their middle zones characterized by $c_F(y,t) = 0.5 \pm 0.05$. In both cases, differences between the profiles obtained from flames C,

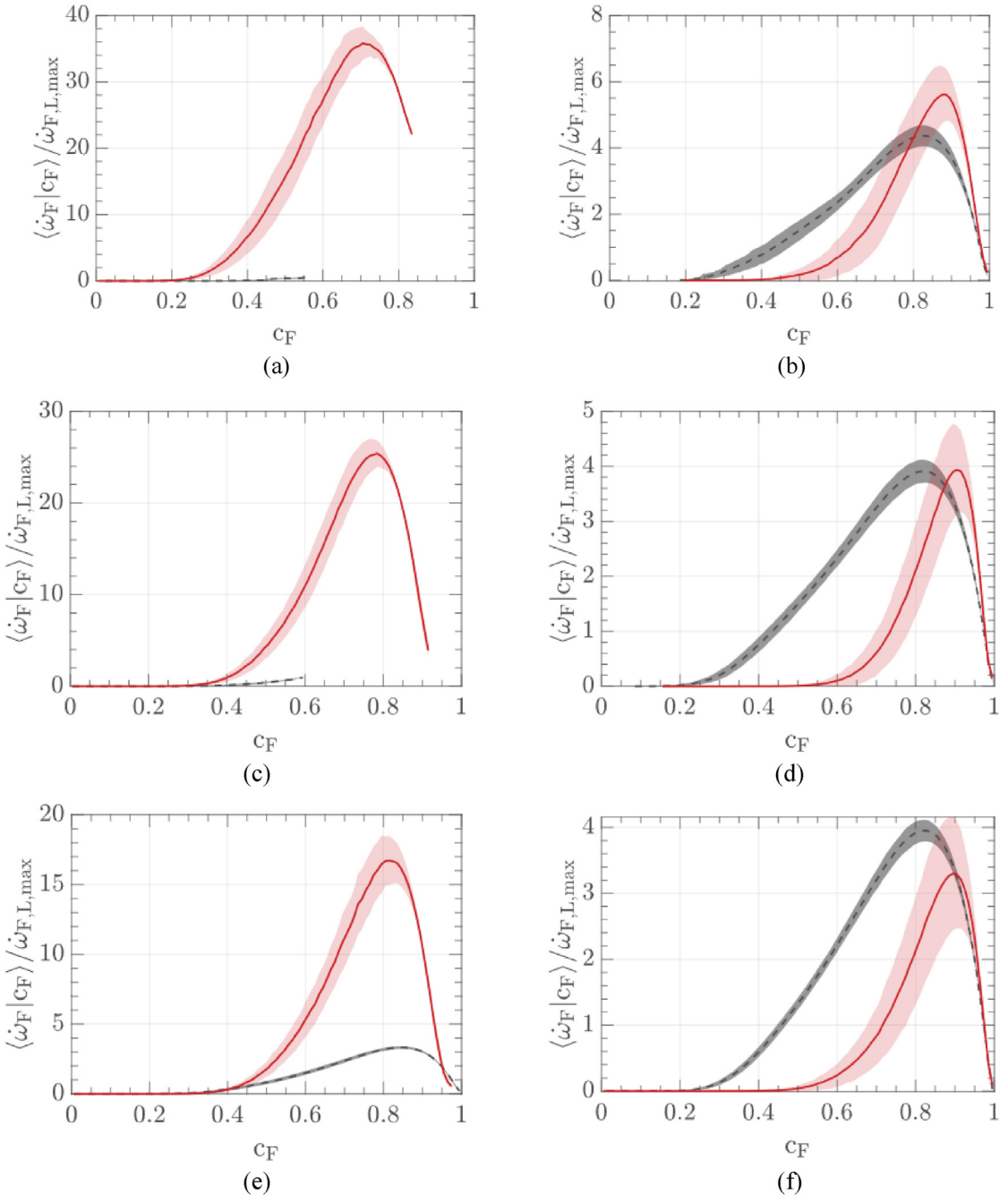

Fig. 5 – Time-averaged conditioned profiles of normalized fuel consumption rate sampled from (a, c, and e) leading and (b, d, and f) trailing edges of flames (a and b) D1H and D1H2, (c and d) E1H and E1H2, and (e and f) F1H and F1H2. Profiles sampled from flames $\mathscr{D}$1H or $\mathscr{D}$1H2 are plotted in black dashed and red solid lines, respectively. The rates are normalized using the peak fuel consumption rate in the unperturbed laminar flame characterized by $\phi = 0.35$. Shaded regions show ± rms values. (For interpretation of the references to color in this figure legend, the reader is referred to the Web version of this article.)

C1, C1H, and C1H2 are quite moderate. These differences are significantly smaller than differences between counterpart conditioned profiles sampled from the flame-brush leading edges, see Fig. 4a. Accordingly, the former differences, see Fig. 9, do not seem to be sufficient to explain the strong influence of molecular transport properties on turbulent burning velocity, as shown in Fig. 7a. Therefore, Figs. 4a, b, 7a, and 9 considered altogether imply that, in line with the leading point concept, significant sensitivity of normalized turbulent burning velocity to the high molecular diffusivity of H_2 is mainly controlled by processes localized to the flame-brush leading edge.

It is worth stressing that magnitude of effects caused by the high molecular diffusivity of H_2 can be extremely high at

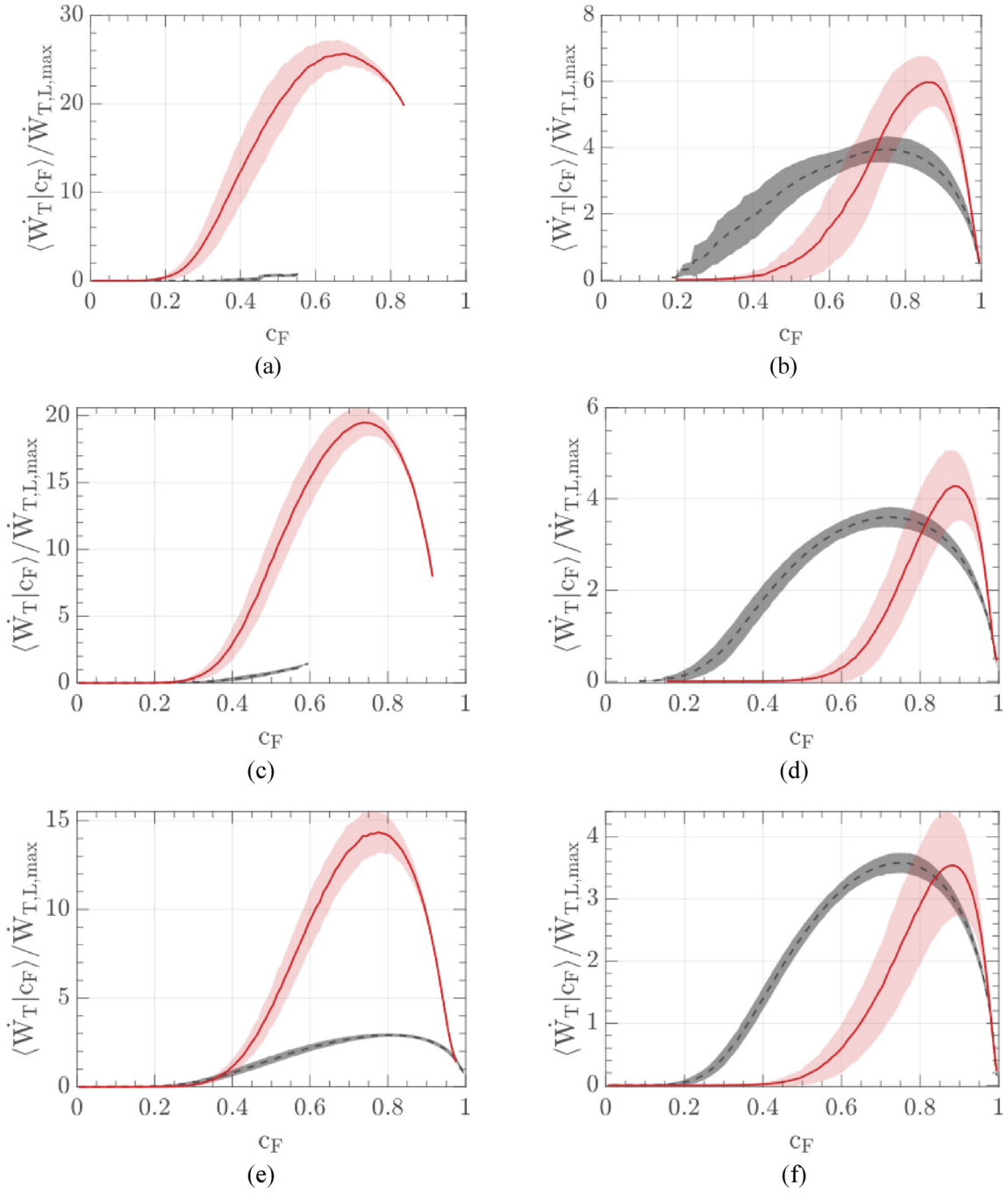

Fig. 6 – Time-averaged conditioned profiles of normalized heat release rate sampled from (a, c, and e) leading and (b, d, and f) trailing edges of flames (a and b) D1H and D1H2, (c and d) E1H and E1H2, and (e and f) F1H and F1H2. Profiles sampled from flames $\mathscr{D}$1H or $\mathscr{D}$1H2 are plotted in black dashed and red solid lines, respectively. The rates are normalized using the peak heat release rate in the unperturbed laminar flame characterized by $\phi = 0.35$. Shaded regions show ± rms values. (For interpretation of the references to color in this figure legend, the reader is referred to the Web version of this article.)

flame-brush leading edge. For instance, Fig. 10 reports time-averaged profiles of the conditioned normalized fuel consumption rate $\overline{\langle \dot{\omega}_F(x,t)/\dot{\omega}_{F,L}[c_F(x,t)]|\dot{\omega}_F(x,t) > 0.1\dot{\omega}_{F,L,max}\rangle}$. Here, normalization is performed (i) using dependencies of $\dot{\omega}_{F,L}(c_F)$, calculated for the unperturbed laminar flames $\mathscr{D}$, and (ii) substituting $c_F = c_F(x,t)$ into these dependencies $\dot{\omega}_{F,L}(c_F)$. Here, $c_F(x,t)$ is the local value of the combustion progress variable in a turbulent flame. The profiles have been sampled from local reaction zones characterized by $\dot{\omega}_F(x,t) > 0.1\dot{\omega}_{F,L,max}$. At the flame-brush leading edges characterized by a low $\langle c_F\rangle(y,t)$, the rate ratio $\dot{\omega}_F(x,t)/\dot{\omega}_{F,L}[c_F(x,t)]$ can reach ten orders of magnitude, see Fig. 10b. While these extremely high ratios are controlled by extremely low $\dot{\omega}_{F,L}[c_F(\mathbf{x},t)]$, whereas $\dot{\omega}_F(x,t) > 0.1\dot{\omega}_{F,L,max}$ due to differential diffusion effects, the

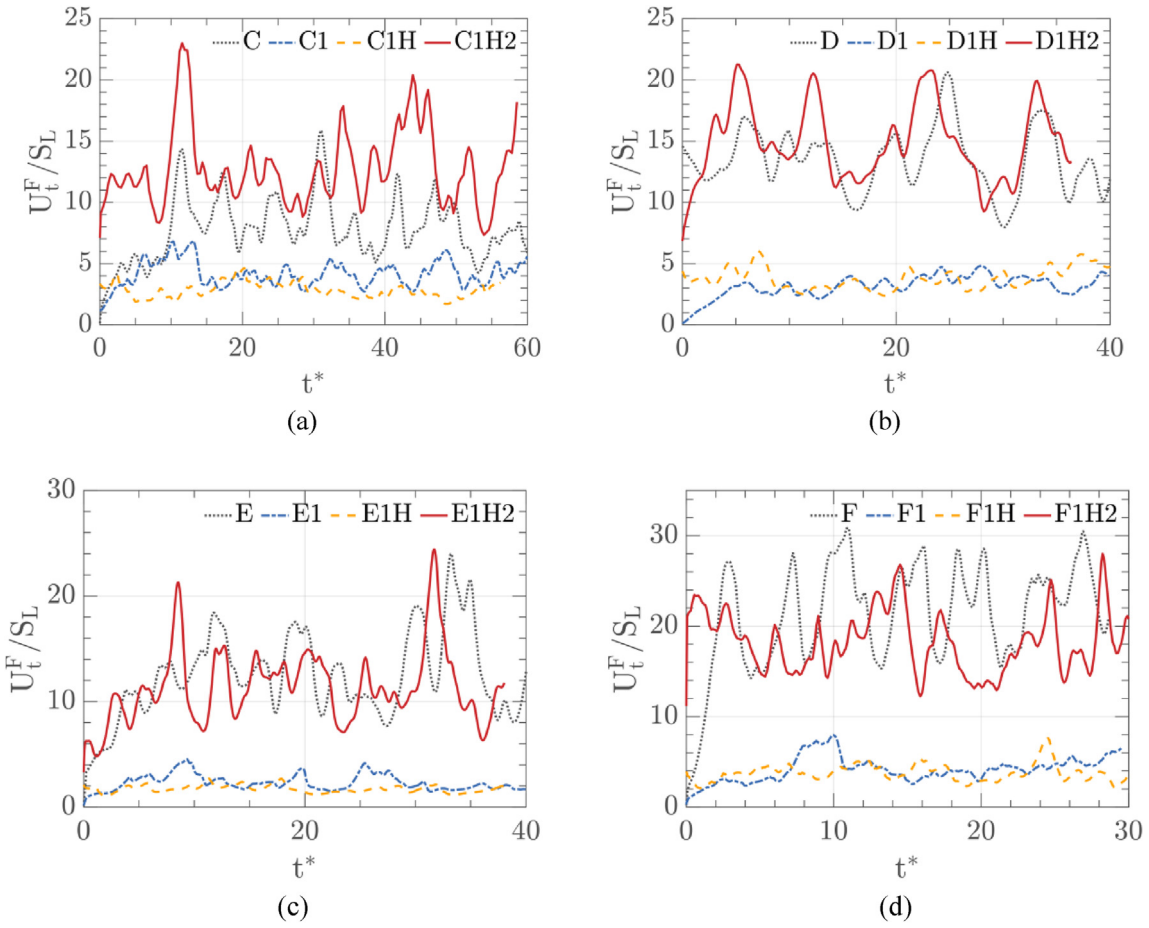

Fig. 7 – Normalized turbulent burning velocities $U_t^F(t^*)/S_L$ obtained from (a) C, (b) D, (c) E, and (d) F sets of flames vs. normalized time $t^* = t/\tau_t$. Cases are specified in figure legends.

documented high magnitude of the rate ratio may appear to be surprising at first glance.

To further support the leading point concept, Fig. 11 reports dependencies of mean normalized fuel consumption rates on mean combustion progress variable, with the normalization being performed using the same $\dot{\omega}_{F,L,max}$ for all four flames $\mathscr{D}$, $\mathscr{D}$1, $\mathscr{D}$1H, and $\mathscr{D}$1H2. Comparison of curves plotted in red solid (cases $\mathscr{D}$1H2) or black dotted (cases $\mathscr{D}$) lines with curves plotted in blue dotted-dashed (cases $\mathscr{D}$1) or yellow dashed (cases $\mathscr{D}$1H) lines shows that high diffusivity of H_2 results in significantly increasing mean fuel consumption rates in the largest parts of the flame brushes, with the effect being most pronounced at their leading edges. For instance, in flame D characterized by the highest *Ka*, the mean fuel consumption rate $\overline{\omega}_{F,D}(\overline{c}_F)$ is much higher than $\overline{\omega}_{F,D1}(\overline{c}_F)$ in flame D1 if $\overline{c}_F < c_F^* = 0.2$ (cf. curves plotted in black dotted and blue dotted-dashed lines in Fig. 11b), with a ratio of the two rates being significantly decreased with increasing $\overline{c}_F$. The effect is even more pronounced when results obtained from flames D1H2 (red solid line) and D1H (yellow dashed line) are compared. The same trends are observed for other sets of flames, but the boundary c_F^* of the leading zone characterized by very high ratios of $\overline{\omega}_{F,\mathscr{D}}/\overline{\omega}_{F,\mathscr{D}1}$ or $\overline{\omega}_{F,\mathscr{D}1H2}/\overline{\omega}_{F,\mathscr{D}1H}$ is decreased with increasing ϕ (cf. Fig. 11a and d) or decreasing *Ka* (cf. Fig. 11b–d).

Note that (i) the peak normalized mean fuel consumption rate is larger than unity in flames D1 and E1, because the peak fuel consumption rate in the laminar flame D-F, used for the normalization, is significantly (by a factor of about 5.5, see Fig. 1c) smaller than the peak fuel consumption rate in the laminar flame D1-F1; and (ii) an increase in the molecular diffusivity of H results in decreasing the mean fuel consumption rate in the largest part of the mean flame brushes, with the exception of their trailing edges (cf. curves plotted in blue dotted-dashed and yellow dashed lines).

Fig. 12 shows that, contrary to the mean fuel consumption rate, mean flame surface density $\overline{|\nabla c_F|}$ is weakly affected by differences in molecular transport coefficients in all four sets of flames. The same trend is observed in Table 3, where time-averaged values of the integral

$$\Sigma_t^F(t) = \frac{1}{L_x^2}\iint_\Omega |\nabla c_F|(x,t)dx \tag{4}$$

are reported. Therefore, the documented significant increase in U_t^F due to high molecular diffusivity of H_2, see Fig. 7 and Table 2, is mainly controlled by an increase in fuel

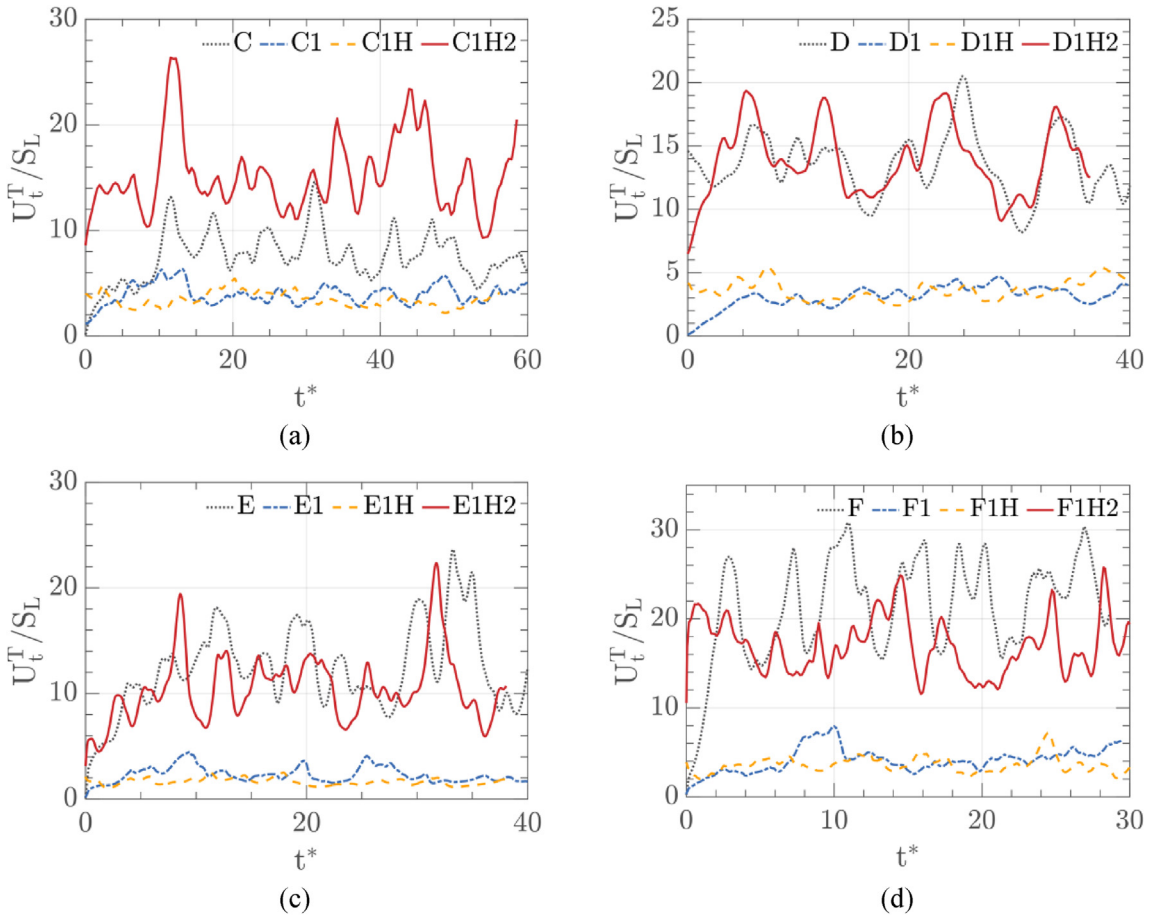

Fig. 8 – Normalized turbulent burning velocities $U_t^T(t^*)/S_L$ obtained from (a) C, (b) D, (c) E, and (d) F sets of flames vs. normalized time $t^* = t/\tau_t$. Cases are specified in figure legends.

Table 2 – Time-averaged mean turbulent burning velocities.

Cases	C	C1	C1H	C1H2	D	D1	D1H	D1H2
$\overline{U_t^F(t^*)}/S_L$	8.2	4.3	2.9	12.6	14.9	3.4	3.8	15.0
$\overline{U_t^T(t^*)}/S_L$	8.0	4.1	2.8	11.9	14.9	3.4	3.6	14.1
Cases	**E**	**E1**	**E1H**	**E1H2**	**F**	**F1**	**F1H**	**F1H2**
$\overline{U_t^F(t^*)}/S_L$	12.6	2.2	1.7	11.7	22.4	4.5	3.8	18.5
$\overline{U_t^T(t^*)}/S_L$	12.6	2.2	1.6	10.9	22.4	4.5	3.6	17.3

consumption rate. A similar result was earlier reported by Chakraborty and Cant [76] who performed DNS of single-step-chemistry turbulent flames characterized by various Lewis numbers. Moreover, since thermo-diffusive instability of a premixed flame results in increasing flame surface area [38,74,75]; in turbulent flames, the instability is often associated with an increase in flame surface density. Accordingly, Fig. 12 does not seem to evidence that the instability plays an important role in the studied turbulent flames. In this regard, it is worth recalling a DNS study of two weakly turbulent ($u'/S_L = 0.72$ and 2.8) V-shaped flames, performed by Day et al. [99]. These authors have noted that "with increasing turbulence levels … fluctuations, at even the lowest intensity levels, appear to suppress to some extent the growth and propagation of the spherical burning cells characteristic of the thermo-diffusive instability" [99, p. 1043]. Moreover, other DNS data [100, fig. 6] show that both length scales and magnitudes of fuel consumption rate perturbations are very different in unstable laminar and turbulent lean H_2/air flames. These significant differences appear also to put into question a hypothesis that thermo-diffusive instability controls the strong influence of differences in molecular transport coefficients on turbulent burning velocity in lean H_2-air mixtures.

In addition to the results discussed above, Figs. 5–8 and Table 2 show other trends that deserve consideration:

- An increase (when compared to the laminar flames) in the fuel consumption or heat release rate due to preferential diffusion of molecular hydrogen is much more pronounced at the leading edges of the leaner turbulent flame brushes D1H2, E1H2, and F1H2 when compared to the richer turbulent flame C1H2, cf. curves plotted in red solid lines in Fig. 1 and in the left columns of Figs. 4–6. In particular,

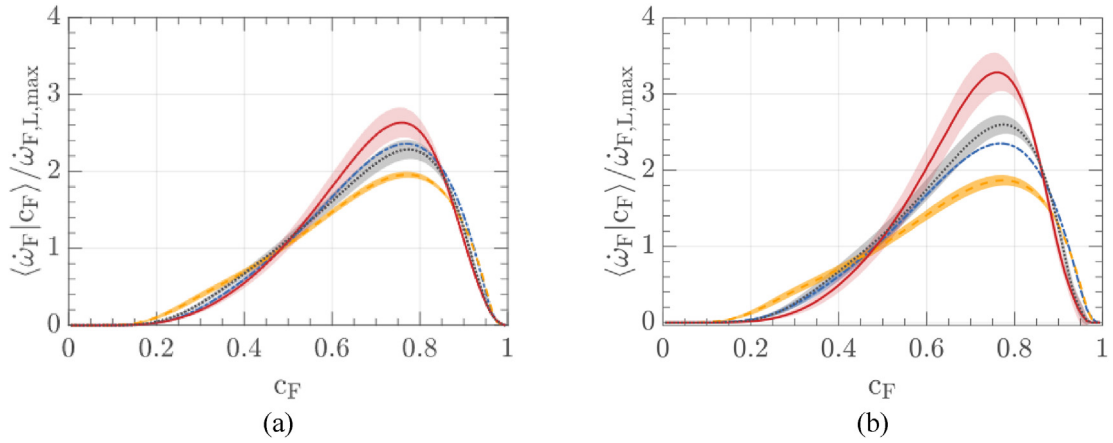

Fig. 9 – Time-averaged conditioned profiles of normalized fuel consumption rate, sampled from (a) entire flame brushes and (b) their middle zones characterized by $c_F(y,t) = 0.5 \pm 0.05$. Black dotted, blue dotted-dashed, yellow dashed, and red solid lines show the profiles sampled from flames C, C1, C1H, and C1H2, respectively. The rates are normalized using the peak fuel consumption rate in the unperturbed laminar flame characterized by $\phi = 0.5$. Shaded regions show ± rms values. (For interpretation of the references to color in this figure legend, the reader is referred to the Web version of this article.)

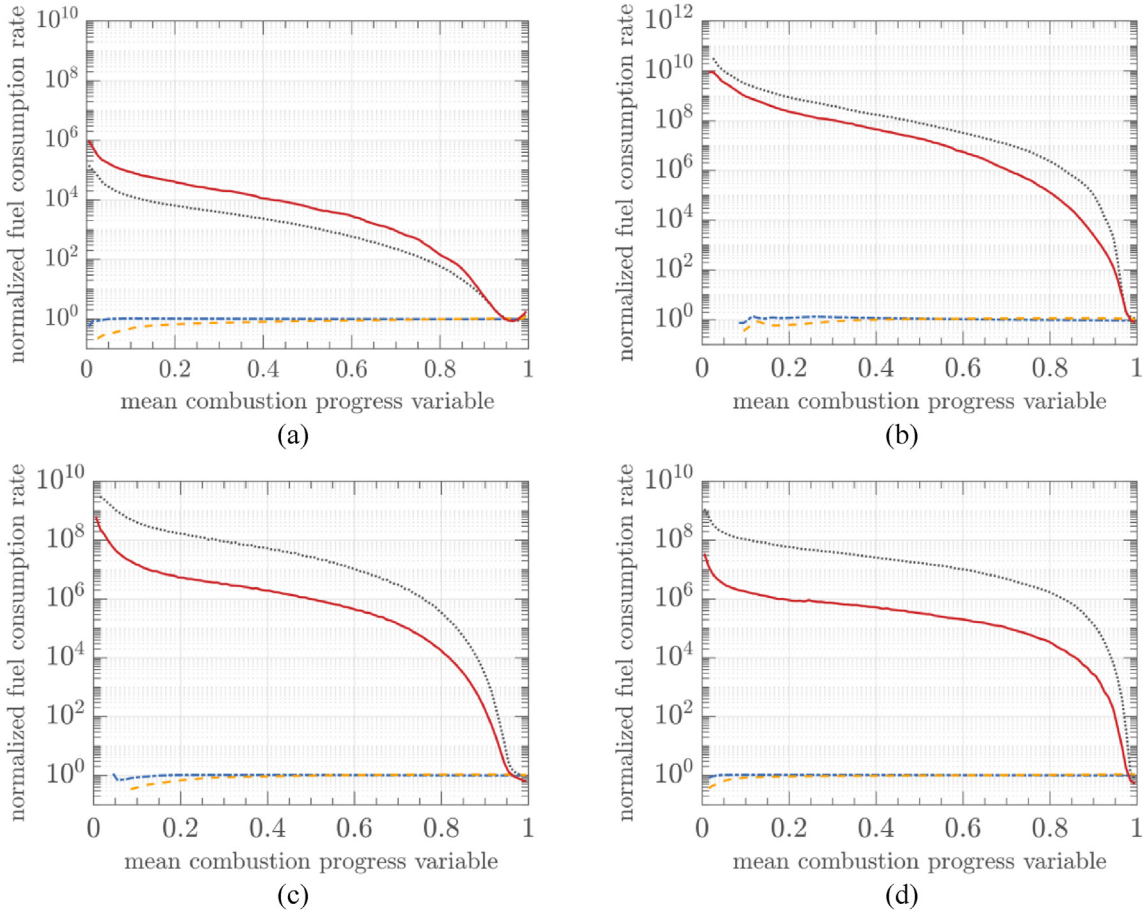

Fig. 10 – Time-averaged conditioned profiles of the fuel consumption rate $\dot{\omega}_F(x,t)$, which is normalized using the unperturbed-laminar-flame fuel consumption rate $\dot{\omega}_{F,L}[c_F(x,t)]$ evaluated at the local value of the combustion progress variable in the turbulent flame. The profiles have been sampled from local reaction zones characterized by $\dot{\omega}_F(x,t) > 0.1\dot{\omega}_{F,L,max}$. Profiles sampled from flames $\mathscr{D}$, $\mathscr{D}$1, $\mathscr{D}$1H, and $\mathscr{D}$1H2 are plotted in black dotted, blue dotted-dashed, yellow dashed, and red solid lines, respectively. (a) C set of flames, (b) D set of flames, (c) E set of flames, and (d) F set of flames. (For interpretation of the references to color in this figure legend, the reader is referred to the Web version of this article.)

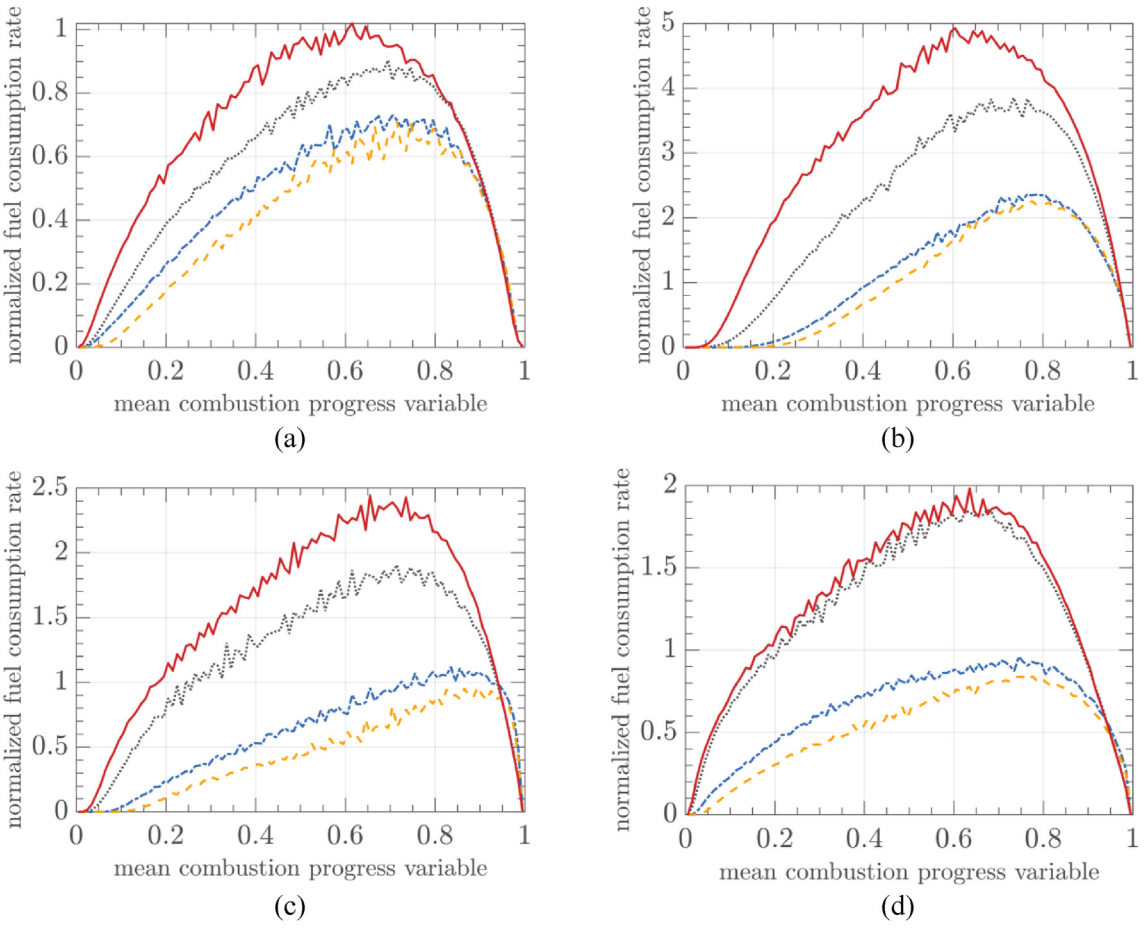

Fig. 11 – Variations of mean normalized fuel consumption rates across flame brushes in (a) C, (b) D, (c) E, and (d) F sets of flames. Results obtained from flames $\mathscr{D}$, $\mathscr{D}$1, $\mathscr{D}$1H, and $\mathscr{D}$1H2 are plotted in black dotted, blue dotted-dashed, yellow dashed, and red solid lines, respectively. In all four cases $\mathscr{D}$, $\mathscr{D}$1, $\mathscr{D}$1H, and $\mathscr{D}$1H2, the normalization is performed using the peak fuel consumption rate $\dot{\omega}_{F,L,max}$ in the unperturbed laminar flame (a) C or (b–d) D. (For interpretation of the references to color in this figure legend, the reader is referred to the Web version of this article.)

ratios of the peak conditioned fuel consumption rates sampled from the turbulent flames at $\langle c_F \rangle(y,t) = 0.1 \pm 0.05$, see Figs. 4a, 5a, c, and e, to the peak fuel consumption rates in the counterpart laminar flames, see Fig. 1a and c, are equal to 4.3, 16.4, 11.8, and 7.7 in cases C1H2, D1H2, E1H2, and F1H2, respectively. For the heat release rates, similar ratios are equal to 3.4, 11.1, 8.7, and 6.4, respectively. These numbers show that the effect magnitude (i) is larger for the fuel consumption rate when compared to the heat release rate and (ii) is decreased with decreasing *Ka*, see Table 1, for the leanest flames D1H2, E1H2, and F1H2.

- An increase (when compared to the counterpart laminar flames) in the fuel consumption or heat release rate due to preferential diffusion of atomic hydrogen is observed at the trailing edges of the studied turbulent flame brushes, see right columns in Figs. 4 and 5, but the effect magnitude is relatively low (for the peak conditioned rates, it is about 20% in case D1H characterized by the highest *Ka* and 10% or less in other $\mathscr{D}$1H cases).
- Influence of differential diffusion on turbulent burning velocity is more pronounced in the leaner mixture. For instance, ratios of $R_U \equiv (\overline{U_t^F}/S_L)_{\mathscr{D}}/(\overline{U_t^F}/S_L)_{\mathscr{D}1}$ are equal to 1.9, 4.4, 5.7, 5.0 for pairs C and C1, D and D1, E and E1, F and F1, respectively. While the major non-dimensional characteristics of premixed turbulent flames are approximately the same in cases C and F, the ratio R_U is significantly larger in the leaner flame F.
- The magnitude of such differential diffusion effects depends weakly on Karlovitz number, cf. R_U for D and F sets of cases and note that $Ka_D/Ka_F \cong 17$. The computed effect of *Ka* on R_U is significantly less than the effect of the equivalence ratio, cf. cases C and F. For the leaner flames D, E, and F, the ratio R_U depends non-monotonously on Karlovitz number. The peak value of $R_U = 5.7$ is reached at $Ka = 53$.
- Under conditions of the present study (intense small-scale turbulence), the normalized turbulent burning velocity $\overline{U_t^F}/S_L$ is significantly increased by the integral length scale *L*, cf. cases E and F in Table 2. The effect magnitude is almost the same for low *Le* and equidiffusive flames, i.e., (i) $\overline{U_t^F}/S_L$ in flame F is larger by a factor about 1.8 than this ratio in flame E and (ii) $\overline{U_t^F}/S_L$ in flame F1 is larger by a factor about 2.2 than $\overline{U_t^F}/S_L$ in flame E1. Note that a significant decrease in burning velocity with decreasing an integral length scale

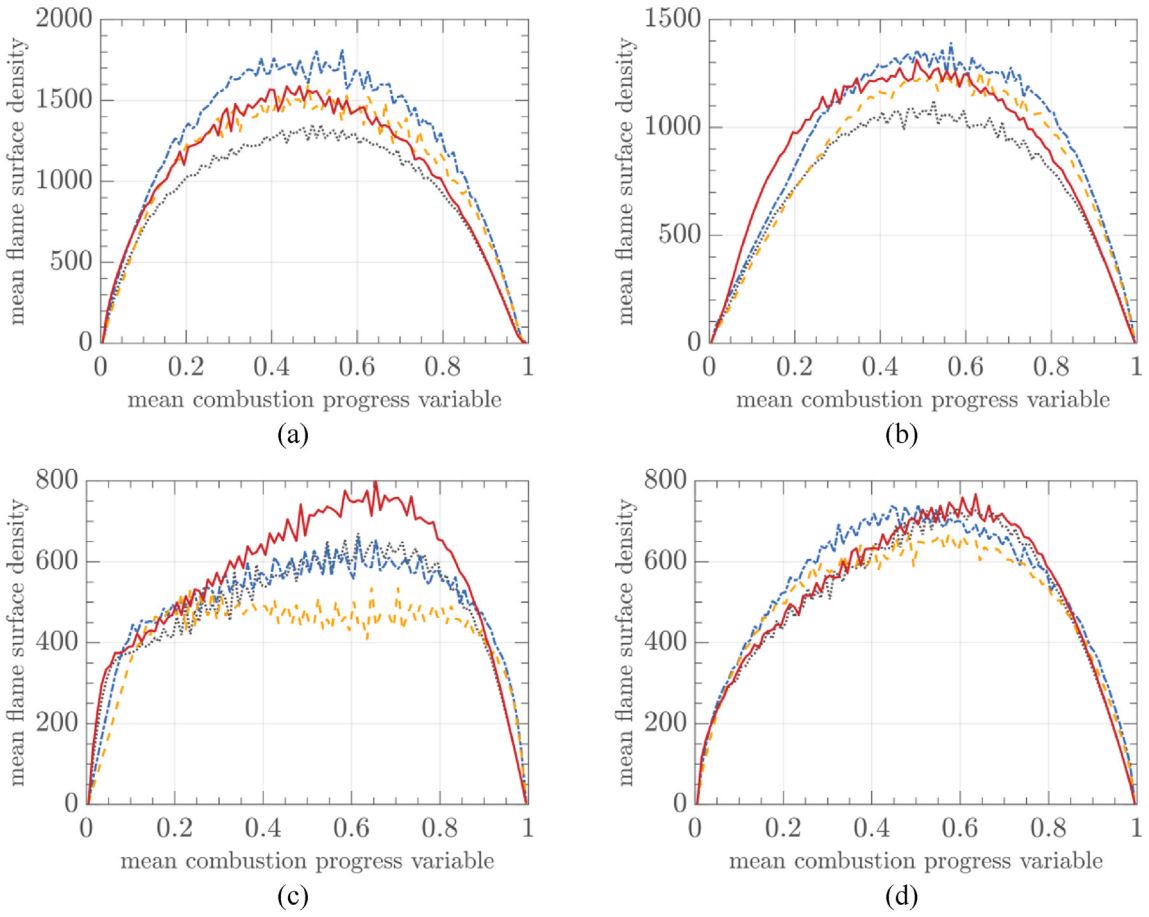

Fig. 12 – Variations of mean flame surface densities across flame brushes in (a) C, (b) D, (c) E, and (d) F sets of flames. Results obtained from flames $\mathscr{D}$, $\mathscr{D}$1, $\mathscr{D}$1H, and $\mathscr{D}$1H2 are plotted in black dotted, blue dotted-dashed, yellow dashed, and red solid lines, respectively. (For interpretation of the references to color in this figure legend, the reader is referred to the Web version of this article.)

Table 3 – Time-averaged integrals $\overline{\Sigma_t^F(t)}$ of mean flame surface density.

C	C1	C1H	C1H2	D	D1	D1H	D1H2	E	E1	E1H	E1H2	F	F1	F1H	F1H2
3.4	4.3	3.3	4.2	2.6	3.5	3.7	2.9	2.3	2.3	1.9	2.8	4.4	4.4	3.7	5.1

of intense small-scale turbulence was also observed [101,102] by analyzing other DNS databases obtained from lean complex-chemistry hydrogen-air flames propagating in spatially decaying turbulence.

Further discussion of the trends listed above is beyond the scope of the present contribution, which aims solely at illuminating an important role played by the leading edge of a premixed turbulent flame brush in its propagation. These trends will be explored in subsequent papers.

Conclusions

Unsteady three-dimensional Direct Numerical Simulation data obtained from 16 statistically planar and one-dimensional, complex-chemistry, lean hydrogen-air flames propagating in forced, intense, small-scale turbulence were analyzed in order to develop a simple numerical method for comparing roles played by leading and trailing edges of a premixed turbulent flame brush in its propagation. The method is based on considerations that (i) positively (negatively) curved reaction zones predominate at the leading (trailing, respectively) edge of a premixed turbulent flame brush and (ii) preferential diffusion of molecular or atomic hydrogen results in increasing the local burning rate in positively or negatively curved reaction zones, respectively. Accordingly, turbulent burning velocities computed by deactivating differential diffusion effects for all species with the exception of either molecular or atomic hydrogen are proposed to be compared for assessing roles played by the leading and trailing edges of a premixed turbulent flame brush in its propagation.

By analyzing the DNS data, the two aforementioned hypotheses are confirmed and a significant increase in the *local*

burning rate due to preferential diffusion of H_2 or H is documented close to the leading or trailing edges, respectively, of the studied flame brushes.

For all simulated sets of flames, the *bulk* turbulent burning velocities computed by activating preferential diffusion solely for H_2 are significantly higher than the *bulk* turbulent burning velocities computed by activating preferential diffusion solely for H.

Moreover, fuel consumption rate is significantly increased due to high molecular diffusivity of H_2, with the effect magnitude being much more pronounced in the vicinity of the flame-brush leading edges. On the contrary, mean flame surface density is weakly affected by variations of molecular diffusivities of H_2 or H.

All these results are fully consistent with leading point concept of premixed turbulent combustion. We are not aware of an alternative approach capable of qualitatively predicting the reported results altogether.

Declaration of competing interest

The authors declare that they have no known competing financial interests or personal relationships that could have appeared to influence the work reported in this paper.

Acknowledgment

This work has been supported in part by NSFC (Grant Nos. 91752201, 51976088, and 92041001), the Shenzhen Science and Technology Program (Grant Nos. KQTD20180411143441009 and JCYJ20210324104802005), Department of Science and Technology of Guangdong Province (Grant Nos. 2019B21203001 and 2020B1212030001), and by project no. LCH-2019011 under the Joint Program of Shenzhen Clean Energy Research Institute and SUSTech through contract CERI-KY-2019-003. AL acknowledges support provided by Combustion Engine Research Center (CERC).

REFERENCES

[1] Kober T, Schiffer HW, Densing M, Panos P. Global energy perspectives to 2060 – WEC's world energy scenarios 2019. Energy Strategy Rev 2020;31:100523.
[2] Acar C, Dincer I. The potential role of hydrogen as a sustainable transportation fuel to combat global warming. Int J Hydrog Energy 2000;45:3396–406.
[3] Bičáková O, Straka P. Production of hydrogen from renewable resources and its effectiveness. Int J Hydrog Energy 2012;37:11563–78.
[4] Dincer I, Acar C. A review on potential use of hydrogen in aviation applications. Int J Sustain Aviat 2016;2:74–100.
[5] Kovač K, Paranos M, Marciuš D. Hydrogen in energy transition: a review. Int J Hydrog Energy 2021;46:10016–35.
[6] Karim GA. Hydrogen as a spark ignition engine fuel. Int J Hydrog Energy 2003;28:569–77.
[7] Verhelst S, Wallner T. Hydrogen-fueled internal combustion engines. Prog Energy Combust Sci 2009;35:490–527.
[8] Yip HL, Srna A, Yuen ACY, Kook S, Taylor RA, Yeoh GH, et al. A review of hydrogen direct injection for internal combustion engines: towards carbon-free combustion. Appl Sci 2019;9:4842.
[9] Choubey GDY, Huang W, Yan L, Babazadeh H, Pandey KM. Hydrogen fuel in scramjet engines – a brief review. Int J Hydrog Energy 2020;45:16799–815.
[10] Stępień Z. A comprehensive overview of hydrogen-fueled internal combustion engines: achievements and future challenges. Energies 2021;14:6504.
[11] Zhang M, Chang M, Wang J, Huang Z. Flame dynamics analysis of highly hydrogen-enrichment premixed turbulent combustion. Int J Hydrog Energy 2020;45:1072–83.
[12] Huang K, Sun ZY, Tian YC, Wang KL. Turbulent combustion evolution of stoichiometric H_2/CH_4/air mixtures within a spherical space. Int J Hydrog Energy 2020;45:10613–22.
[13] Liu X, Bertsch M, Subash AA, Yu S, Szasz RZ, Li Z, et al. Investigation of turbulent premixed methane/air and hydrogen-enriched methane/air flames in a laboratory-scale gas turbine model combustor. Int J Hydrog Energy 2021;46:13377–88.
[14] Öberg S, Odenberger M, Johnsson F. Exploring the competitiveness of hydrogen-fueled gas turbines in future energy systems. Int J Hydrog Energy 2021;46:624–44.
[15] Yakovenko IS, Ivanov MF, Kiverin AD, Melnikova KS. Large-scale flame structures in ultra-lean hydrogen-air mixtures. Int J Hydrog Energy 2018;43:1894–901.
[16] Ghiasi G, Doan NAK, Swaminathan S, Yenerdag B, Minamoto Y, Tanahashi M. Assessment of SGS closure for isochoric combustion of hydrogen-air mixture. Int J Hydrog Energy 2018;43:8105–15.
[17] Gavrikov AI, Golub VV, Mikushkin AY, Petukhov VA, Volodin VV. Lean hydrogen-air premixed flame with heat loss. Int J Hydrog Energy 2019;44:20462–9.
[18] Minamoto Y, Tanahashi M. Effect of turbulent motions at different length scales on turbulent premixed swirl-stabilised flame topology. Int J Hydrog Energy 2019;44:22316–27.
[19] Sun H, Yan P, Xu Y. Numerical simulation on hydrogen combustion and flow characteristics of a jet-stabilized combustor. Int J Hydrog Energy 2020;45:12604–15.
[20] Yakovenko IS, Kiverin AD. Intensification mechanisms of the lean hydrogen-air combustion via addition of suspended micro-droplets of water. Int J Hydrog Energy 2021;46:1259–72.
[21] Shan F, Zhang D, Hou L, Fang H, Zhang H, Zhang J. An improved flamelet/progress variable modeling for supersonic combustion. Int J Hydrog Energy 2021;46:4485–95.
[22] Gao W, Yan Y, Huang L, Zhang W, Shen K. Numerical investigation on combustion characteristics of premixed hydrogen/air in a swirl micro combustor with twisted vanes. Int J Hydrog Energy 2021;46:40105–19.
[23] Babayev R, Andersson A, Dalmau AS, Im HG, Johansson B. Computational characterization of hydrogen direct injection and nonpremixed combustion in a compression-ignition engine. Int J Hydrog Energy 2021;46:18678–96.
[24] Duva BC, Toulson E. Unstretched unburned flame speed and burned gas Markstein length of diluted hydrogen/air mixtures. Int J Hydrog Energy 2022;47:9030–44.
[25] Karpov VP, Sokolik AS. Ignition limits in turbulent gas mixtures. Proc Acad Sci USSR Phys Chem 1961;141:866–9.
[26] Karpov VP, Severin ES. Effects of molecular-transport coefficients on the rate of turbulent combustion. Combust Explos Shock Waves 1980;16:41–6.
[27] Wu MS, Kwon A, Driscoll J, Faeth GM. Turbulent premixed hydrogen/air flames at high Reynolds numbers. Combust Sci Technol 1980;73:327–50.

[28] Abdel-Gayed RG, Bradley D, Hamid MN, Lawes M. Lewis number effects on turbulent burning velocity. Proc Combust Inst 1984;20:505–12.
[29] Kido H, Nakahara M. A model of turbulent burning velocity taking the preferential diffusion effect into consideration. JSME Int J 1998;41:666–73.
[30] Daniele S, Jansohn P, Mantzaras J, Boulouchos K. Turbulent flame speed for syngas at gas turbine relevant conditions. Proc Combust Inst 2011;33:2937–44.
[31] Venkateswaran P, Marshall A, Shin DH, Noble D, Seitzman J, Lieuwen T. Measurements and analysis of turbulent consumption speeds of H_2/CO mixtures. Combust Flame 2011;158:1602–14.
[32] Venkateswaran P, Marshall A, Seitzman J, Lieuwen T. Pressure and fuel effects on turbulent consumption speeds of H_2/CO blends. Proc Combust Inst 2013;34:1527–35.
[33] Yang S, Saha A, Liang W, Wu F, Law CK. Extreme role of preferential diffusion in turbulent flame propagation. Combust Flame 2018;188:498–504.
[34] Lipatnikov AN, Chomiak J. Molecular transport effects on turbulent flame propagation and structure. Prog Energy Combust Sci 2005;31:1–73.
[35] Lipatnikov AN. Fundamentals of premixed turbulent combustion. CRC Press; 2012.
[36] Karpov V, Lipatnikov A, Zimont V. A test of an engineering model of premixed turbulent combustion. Proc Combust Inst 1996;26:249–57.
[37] Karpov VP, Lipatnikov AN, Zimont VL. Flame curvature as a determinant of preferential diffusion effects in premixed turbulent combustion [chapter 14]. In: Sirignano WA, Merzhanov AG, de Luca L, editors. Advances in combustion science: in honor of Ya.B. Zel'dovich, vol. 173. Prog Astronaut Aeronautics; 1996. p. 235–50.
[38] Zel'dovich YaB, Barenblatt GI, Librovich VB, Makhviladze GM. The mathematical theory of combustion and explosions. Consultants Bureau; 1985.
[39] Kuznetsov VR, Sabelnikov VA. Turbulence and combustion. Hemisphere; 1990.
[40] Fisher RA. The wave of advance of advantageous genes. Ann Eugen 1937;7:355–69.
[41] Kolmogorov AN, Petrovsky I, Piskounov N. A study of the diffusion equation with a source term and its application to a biological problem. Bjull MGU A 1937;1(6):1–26 (English translation in Pelcé P, editor. Dynamics of curved fronts. Academic Press; 1988. pp. 105–130).
[42] Ebert U, van Saarloos W. Front propagation into unstable states: universal algebraic convergence towards uniformly translating pulled fronts. Physica D 2000;146:1–99.
[43] van Saarloos W. Front propagation into unstable states. Phys Rep 2003;386:29–222.
[44] Murray JD. Lectures on nonlinear-differential-equation models in biology. Clarendon Press; 1977.
[45] Murray JD. Mathematical biology 1. An introduction. 3rd ed. Springer; 2002.
[46] Bray KNC, Libby PA. Interaction effects in turbulent premixed flames. Phys Fluids 1976;19:1687–701.
[47] Hakberg B, Gosman AD. Analytical determination of turbulent flame speed from combustion models. Proc Combust Inst 1984;20:225–32.
[48] Libby PA. Theory of normal premixed turbulent flames revisited. Prog Energy Combust Sci 1985;11:83–96.
[49] Bray KNC. Studies of the turbulent burning velocity. Proc R Soc Lond A 1990;431:315–35.
[50] Catlin CA, Lindstedt RP. Premixed turbulent burning velocities derived from mixing controlled reaction models with cold front quenching. Combust Flame 1991;85:427–39.
[51] Duclos J, Veynante D, Poinsot T. A comparison of flamelet models for premixed turbulent combustion. Combust Flame 1993;95:101–18.
[52] Choi CR, Huh KY. Development of a coherent flamelet model for spark-ignited turbulent premixed flame in a closed vessel. Combust Flame 1998;114:336–48.
[53] Kolla H, Rogerson JW, Chakraborty N, Swaminathan N. Scalar dissipation rate modeling and its validation. Combust Sci Technol 2009;181:518–35.
[54] Kolla H, Rogerson JW, Swaminathan N. Validation of a turbulent flame speed model across combustion regimes. Combust Sci Technol 2010;182:284–308.
[55] Zhang W, Wang J, Yu Q, Jin W, Zhang M, Huang Z. Investigation of the fuel effects on burning velocity and flame structure of turbulent premixed flames based on leading points concept. Combust Sci Technol 2018;190:1354–76.
[56] Sabelnikov VA, Lipatnikov AN. Transition from pulled to pushed premixed turbulent flames due to countergradient transport. Combust Theor Model 2013;17:1154–75.
[57] Sabelnikov VA, Lipatnikov AN. Transition from pulled to pushed fronts in premixed turbulent combustion: theoretical and numerical study. Combust Flame 2015;162:2893–903.
[58] Kha KQN, Robin V, Mura A, Champion M. Implications of laminar flame finite thickness on the structure of turbulent premixed flames. J Fluid Mech 2016;787:116–47.
[59] Kim SH. Leading points and heat release effects in turbulent premixed flames. Proc Combust Inst 2017;36:2017–24.
[60] Dave HL, Mohan A, Chaudhuri S. Genesis and evolution of premixed flames in turbulence. Combust Flame 2018;196:386–99.
[61] Lipatnikov AN, Chakraborty N, Sabelnikov VA. Transport equations for reaction rate in laminar and turbulent premixed flames characterized by non-unity Lewis number. Int J Hydrog Energy 2018;43:21060–9.
[62] Verma S, Monnier F, Lipatnikov AN. Validation of leading point concept in RANS simulations of highly turbulent lean syngas-air flames with well-pronounced diffusional-thermal effects. Int J Hydrog Energy 2021;46:9222–33.
[63] Lipatnikov AN, Chomiak J. Dependence of heat release on the progress variable in premixed turbulent combustion. Proc Combust Inst 2000;28:227–34.
[64] Aronson DG, Weinberger HF. Nonlinear diffusion in population genetics, combustion, and nerve pulse propagation. In: Goldstein JA, editor. Partial differential equations and related topics. vol. 446; 1975. p. 5–49.
[65] Sabelnikov VA, Petrova NN, Lipatnikov AN. Analytical and numerical study of travelling waves using the Maxwell-Cattaneo relaxation model extended to reaction-advection-diffusion systems. Phys Rev E 2016;94:42218.
[66] Hadeler KP, Rothe F. Travelling fronts in nonlinear diffusion equations. J Math Biol 1975;2:251–63.
[67] Zel'dovich YaB, Frank-Kamenetsky DA. A theory of thermal flame propagation. Acta Physicochem URSS 1938;9:341–6.
[68] Aldushin AP, Zel'dovich YaB, Khudyaev SI. Numerical investigation of flame propagation in a mixture reacting at the initial temperature. Combust Explos Shock Waves 1979;15:705–10.
[69] YaB Zel'dovich. Regime classification of an exothermic reaction with nonuniform initial conditions. Combust Flame 1980;39:211–4.
[70] YaB Zel'dovich. Flame propagation in a substance reacting at initial temperature. Combust Flame 1980;39:219–24.
[71] Clavin P, Linān A. Theory of gaseous combustion. In: Velarde MG, editor. Nonequilibrium cooperative

phenomena in physics and related fields. NATO ASI Series, vol. 116; 1984. p. 291–338.
[72] Gruber A, Bothien MR, Ciani A, Aditya K, Chen JH, Williams FA. Direct numerical simulation of hydrogen combustion at auto-ignitive conditions: ignition, stability and turbulent reaction-front velocity. Combust Flame 2021;229:111385.
[73] Rieth M, Gruber A, Williams FA, Chen JH. Enhanced burning rates in hydrogen-enriched turbulent premixed flames by diffusion of molecular and atomic hydrogen. Combust Flame 2022;239:111740. https://doi.org/10.1016/j.combustflame.2021.111740.
[74] Clavin P. Dynamical behavior of premixed flame fronts in laminar and turbulent flows. Prog Energy Combust Sci 1985;11:1–59.
[75] Matalon M. Flame dynamics. Proc Combust Inst 2009;32:57–82.
[76] Chakraborty N, Cant RS. Effects of Lewis number on turbulent scalar transport and its modelling in turbulent premixed flames. Combust Flame 2009;156:1427–44.
[77] Chakraborty N, Konstantinou I, Lipatnikov AN. Effects of Lewis number on vorticity and enstrophy transport in turbulent premixed flames. Phys Fluids 2016;28:15109.
[78] Aspden AJ, Day MJ, Bell JB. Lewis number effects in distributed flames. Proc Combust Inst 2011;33:1473–80.
[79] Aspden AJ, Day MJ, Bell JB. Turbulence-flame interactions in lean premixed hydrogen: transition to the distributed burning regime. J Fluid Mech 2011;680:287–320.
[80] Day M, Tachibana S, Bell J, Lijewski M, Beckner V, Cheng RK. A combined computational and experimental characterization of lean premixed low swirl laboratory flames II. Hydrogen flames. Combust Flame 2015;162:2148–65.
[81] Carlsson H, Yu R, Bai XS. Direct numerical simulation of lean premixed CH_4/air and H_2/air flames at high Karlovitz numbers. Int J Hydrog Energy 2014;39:20216–32.
[82] Aspden AJ, Day MS, Bell JB. Turbulence-chemistry interaction in lean premixed hydrogen combustion. Proc Combust Inst 2015;35:1321–9.
[83] Aspden AJ, Day MJ, Bell JB. Towards the distributed burning regime in turbulent premixed flames. J Fluid Mech 2019;871:1–21.
[84] Lee HC, Dai P, Wan M, Lipatnikov AN. A DNS study of extreme and leading points in lean hydrogen-air turbulent flames – part I: local thermochemical structure and reaction rates. Combust Flame 2022;235:111716.
[85] Williams FA. Progress in knowledge of flamelet structure and extinction. Prog Energy Combust Sci 2000;26:657–82.
[86] Veynante D, Duclos JM, Piana J. Experimental analysis of flamelet models for premixed turbulent combustion. Proc Combust Inst 1994;25:1249–56.
[87] Ashurst WT, Shepherd IG. Flame front curvature distributions in turbulent premixed flame zone. Combust Sci Technol 1997;124:115–44.
[88] Kostiuk LW, Shepherd IG, Bray KNC. Experimental study of premixed turbulent combustion in opposed streams. Part III – spatial structure of flames. Combust Flame 1999;118:129–39.
[89] Trouvé A, Poinsot T. Evolution equation for flame surface density in turbulent premixed combustion. J Fluid Mech 1994;278:1–31.
[90] Jenkins KW, Cant RS. Curvature effects on flame kernels in a turbulent environment. Proc Combust Inst 2002;29:2023–9.
[91] Sabelnikov VA, Lipatnikov AN, Nishiki S, Dave HL, Hernández-Pérez FE, Song W, et al. Dissipation and dilatation rates in premixed turbulent flames. Phys Fluids 2021;33:35112.
[92] Lee HC, Dai P, Wan M, Lipatnikov AN. A DNS study of extreme and leading points in lean hydrogen-air turbulent flames – part II: local velocity field and flame topology. Combust Flame 2022;235:111712.
[93] Lee HC, Dai P, Wan M, Lipatnikov AN. Influence of molecular transport on burning rate and conditioned species concentrations in highly turbulent premixed flames. J Fluid Mech 2021;298:A5.
[94] Kéromnès A, Metcalfe WK, Heufer KA, Donohoe N, Das AK, Sung CJ, et al. An experimental and detailed chemical kinetic modeling study of hydrogen and syngas mixture oxidation at elevated pressures. Combust Flame 2013;160:995–1011.
[95] Abdelsamie A, Fru G, Oster T, Dietzsch F, Janiga G, Thévenin D. Towards direct numerical simulations of low-Mach number turbulent reacting and two-phase flows using immersed boundaries. Comput Fluids 2016;131:123–41.
[96] Bobbitt B, Lapointe S, Blanquart G. Vorticity transformation in high Karlovitz number premixed flames. Phys Fluids 2016;28:15101.
[97] Bobbitt B, Blanquart G. Vorticity isotropy in high Karlovitz number premixed flames. Phys Fluids 2016;28:105101.
[98] Goodwin D, Malaya N, Moffat H, Speth R. Cantera: an object-oriented software toolkit for chemical kinetics, thermodynamics, and transport processes. Pasadena, CA: Caltech; 2009.
[99] Day MS, Bell JB, Bremer PT, Pascucci V, Beckner VE, Lijewski MJ. Turbulence effects on cellular burning structures in lean premixed hydrogen flames. Combust Flame 2009;156:1035–45.
[100] Day M, Bell JB, Cheng RK, Tachibana S, Beckner V, Lijewski MJ. Cellular burning in lean premixed turbulent hydrogen-air flames: coupling experimental and computational analysis at the laboratory scale. J Phys Conf Ser 2009;180:12031.
[101] Lipatnikov AN, Sabelnikov VA, Hernández-Pérez FE, Song W, Im HG. A priori DNS study of applicability of flamelet concept to predicting mean concentrations of species in turbulent premixed flames at various Karlovitz numbers. Combust Flame 2020;222:370–82.
[102] Song W, Hernández-Pérez FE, Tingas EA, Im HG. Statistics of local and global flame speed and structure for highly turbulent H_2/air premixed flames. Combust Flame 2021;232:111523.